Journal of the Taiwan Institute of Chemical Engineers

Highly effective Pd/ZSM-12 bifunctional catalysts by in-situ glow discharge plasma reduction: the effect of metal function on the catalytic performance for n-hexadecane hydroisomerization
--Manuscript Draft--

Journal of the Taiwan Institute of Chemical Engineers
Submission Checklist

Please check the following points before approving the pdf file for your manuscript. Manuscripts that do not conform may be returned for correction and resubmission. You should be able to answer "yes" to all of the following questions.

1. Is the manuscript double–spaced with a font size of 12 pt (Times or Times New Roman preferred)? ___Yes___

2. Have you given full addresses and affiliations for all co–authors? __ Yes __

3. Is the corresponding author identified by * and contact details (phone number and e–mail address) given on the first page? ___ Yes ___

4. Have you given a "Graphical Abstract" and "Highlights" of your manuscript? __ Yes ___

5. Does the manuscript include a one-paragraph abstract of no more than 200 words for Original Papers or 150 words for Short Communications? ___ Yes ___

6. Do the length of manuscript and the number of display items obey the requirement? ___ There are 10 display items (2 tables and 8 figures) in our manuscript, and about 5000 words and 1400 words in length are included in the main text and references, respectively ___

7. Have keywords (maximum 6) been provided immediately after the abstract? ___ Yes ___

8. Are sections given Arabic numbers with subsections numbered using the decimal system? NOTE: Acknowledgements and References sections are **not** numbered. ___ Yes ___

9. Do you embed all figures, tables, and schemes (including the captions) at appropriate places in the text? ___ Yes ____

10. Are References in the correct format for this journal? __ Yes ____

11. Are all references mentioned in the Reference list cited in the text, and vice versa? ___ Yes ___

12. Has the manuscript been 'spell-checked' and 'grammar-checked'? ___ Yes ___

13. Are all symbols translated correctly in the pdf file? ___ Yes ___

14. Have the written permissions been obtained and uploaded as Additional Files for use of copyrighted materials from other sources (including illustrations, tables, text quotations, Web content, etc.)? Has the copyright information been included in the relevant figure caption or table footnote, as an example "Reprinted with permission from Ref. [10]. Copyright 2010 Elsevier"? ___ Yes ___

Responses to the Comments

We thank the Reviewers for their very helpful comments. We have made revisions and corrections according to the reviewers' comments and suggestions. We have marked all the changes in RED in the revised manuscript. We would like to make the following responses to the comments.

Reviewer #1:

Comment: (1) Should clarify the determination of the total number of acid sites! Why not use NH$_3$-TPD method?

Author reply:

Response: Thanks very much for the comment. In the experimental part of our manuscript, we clarified the determination of the total number of Brønsted acid sites by the IR spectroscopy of the adsorbed pyridine (Py-IR) method, which is the active center for skeleton isomerism of *n*-alkane. (Page 9 line 6-9) We agree with the reviewer's point, and added relevant content about methods for determination and calculation of Lewis acid sites in the experimental section and the results in the support information (the sum of the Brønsted and Lewis acid sites is the total number of acid sites).

In our research work, we also determined the total number of acid sites of ZSM-12 zeolite by using NH$_3$-TPD method, the result is shown in Figure R1 (NH$_3$-TPD experiments were performed on a conventional setup equipped with a thermal conductivity detector and in a argon flow (40 mL/min) and a temperature range from 120 to 650 °C at a heating rate of 10 °C/min.). It can be seen from Figure R1 that the NH$_3$-TPD curve showed signal peaks corresponding to the desorption of NH$_3$ from the weak and strong acid sites at 184 °C and 375 °C, respectively, and the number of weak acid and strong acid sites were 180 μmol/g and 250 μmol/g, respectively.
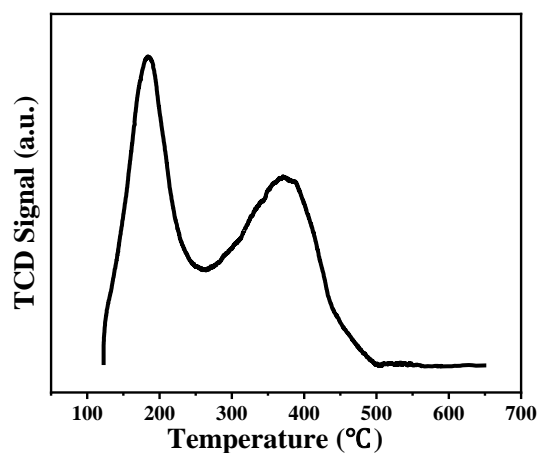
Fig. R1 NH$_3$-TPD curve of ZSM-12 zeolite

Since the active sites that catalyze the skeletal isomerization of *n*-alkanes in the hydroisomerization reaction are Brønsted acid sites, the number of total Brønsted acid sites measured by the Py-IR method is more meaningful for establishing the relationship between acidity, C_{Pd}/C_{H^+} and catalytic performance [1,2] (J Catal 2015;322:1-13 and J Catal 2015;330:485-496). The NH$_3$-TPD method can only give the information about the amount of strong acid and weak acid sites, but cannot give the amount of Brønsted acid sites. Therefore, the

NH₃-TPD method is not used to measure the acid site density of the catalysts in the manuscript.

Action: According to the reviewer's suggestion, we supplemented the related content about the determination of Lewis acid sites by Py-IR method in the experimental section, and added the results of Lewis acid sites in the Table S1 in the SI. In the experimental section of revised manuscript, the method for determining and calculating the number of Brønsted and Lewis acid sites by Py-IR method is marked in RED. The revised content is as follows: "The total and strong Brønsted acid site density was investigated based on the area of the band at approximately 1545 cm⁻¹ in the IR spectra recorded during the desorption of pyridine at 200 °C and 350 °C, respectively. The total Lewis acid sites density was also determined by Py-IR method based on the area of the band at 1545 cm⁻¹. For quantification, the corresponding extinction coefficient of 1.67 cm/μmol and 2.22 cm/μmol for Brønsted and Lewis acid sites was employed, respectively [41,42]." (Page 9 line 6-12) Table S1 was supplemented to the SI section is as follows:

Table S1 The acid sites density of ZSM-12 zeolite and all Pd/Z12 catalysts.

Sample	BAS[a] (C_{H+}, μmol g⁻¹)	LAS[b] (μmol g⁻¹)	TAS[c] (μmol g⁻¹)	BAS Distribution[d] (%)
ZSM-12	23.5	27.3	50.8	56.3
0.1Pd/Z12-C	22.0	26.2	48.2	59.3
0.3Pd/Z12-C	20.5	25.1	45.6	49.9
0.1Pd/Z12-E	21.1	25.4	46.5	53.9
0.3Pd/Z12-E	18.1	23.3	41.4	49.7

[a] Brønsted acid sites, [b]Lewis acid sites, [c]Total acid sites, [d]Distribution of Brønsted acid sites in the total acid sites.

Comment: (2) Should be further analyzed the control in thermodynamic and dynamic range?
Author reply:

Response: Thanks a lot for the comment. According to the reviewer's suggestion, we further analyzed the variation in activity of different catalysts and *iso*-C₁₆ yield obtained in the thermodynamic and dynamic control range, and supplemented some experimental data.

Action:

In the manuscript we have added the following contents about the catalytic reaction laws in the dynamic and thermodynamic control range, respectively.

1. Added the following to the section for explaining catalytic activity:

(1) "Therefore, in the dynamic controlled range, skeletal isomerization and cracking reactions on the acid sites of the bifunctional catalysts are the rate-controlling steps of the reaction, and the Brønsted acid density is the main influence factor of the activity of the bifunctional catalysts." (Page 20 line 15-18)

(2) "Therefore, in the thermodynamic controlled range, when the metal site density of the catalyst is insufficient, the catalytic dehydrogenation of *n*-alkanes and the hydrogenation of *iso*-alkenes intermediates on the metal sites are the rate-controlling steps for the hydroisomerization of *n*-alkanes, and the density of exposed Pd active sites has more importent influence to the activity of the bifunctional catalysts." (Page 21 line 7- Page 22 line 3)

2. Added the following to the section for explaining *iso*-hexadecane yield：

(1) "From Figure 6a, although the 0.3Pd/Z12-E catalyst has the lowest activity among all catalysts at the same tempereture, there is no significant difference in *iso*-hexadecane yield when the *n*-hexadecane conversion is lower than ~20 % (in dynamic controlled range), except for the 0.1Pd/Z12-C catalyst with minimum matal sites density. The low *iso*-hexadecane yield over the 0.1Pd/Z12-C catalyst can be explained by its maximum n_{as} value of 2.28, which represents the average number of acid sites of one *n*-hexadecane molecule contacted during the hydroisomerization reaction between two adjacent metal sites, calculated based on the reaction results at *n*-hexadecane conversion of ~20 % (Table S2). It is found that the n_{as} value of the 0.1Pd/Z12-C catalyst is greater than that of 0.3Pd/Z12-C (1.87), 0.1Pd/Z12-E (1.66) and 0.3Pd/Z12-E (1.48), indicating that stronger cracking reactions even appeared at lower temperatures (corresponding conversion is less than ~20 %) when the metal sites are severely deficient. It is worth noting that, there is a greater difference in the *iso*-hexadecane yield over two series of catalysts in thermodynamic controlled range (at *n*-hexadecane conversion of 80~95 %)." (Page 23 line 1- Page 24 line 5)

(2) "For the *x*Pd/Z12-E series of catalysts, the *iso*-hexadecane yield is also significantly improved when Pd loading increases from 0.1 wt.% to 0.3 wt.%, as well as the C_{Pd}/C_{H+} ratio correspondingly increases from 0.053 to 0.345. The *x*Pd/Z12-E series of catalysts present obviously higher maximum *iso*-hexadecane yield than that of *x*Pd/Z12-C catalysts with same Pd loading at conversion of ~95%, which can be explained by the following reasons. First, *x*Pd/Z12-E catalysts have larger Pd sites density and C_{Pd}/C_{H+} ratio, which is 1.7~2.1 times more than that of *x*Pd/Z12-C series of catalysts with the same Pd loading, which will facilitate hydrogenation of *iso*-alkene intermediates to *iso*-hexadecane rather than further cracking into light hydrocarbons. Furthermore, *x*Pd/Z12-E catalysts expose more Pd (111) facets because of the kinetically controlled growth mechanism for the Pd nanoparticles, which leads to a much stronger H_2 chemical adsorption and dissociation capacity compared with *x*Pd/Z12-C series catalysts with exposure of more Pd (100) facets [58]." (Page 24 line 15 - Page 25 line 6)

3. n_{as} value of all catalysts are added to the Table S2, which were used to explain the law of *iso*-C_{16} yield on each catalyst when the conversion of *n*-C_{16} is lower than 20% (dynamic control range).

Table S2. Calculated n_{as} value of all Pd/Z12 catalysts at *n*-hexadecane conversion of about 20 %.

Catalysts	M	B	C	Nc[d]	n_{as}[e]
0.1Pd/Z12-C	0.58[a]	0.13[a]×2.5[b]=0.33	0.29[a]×4.74[c]=1.37	3.48	2.28
0.3Pd/Z12-C	0.71[a]	0.09[a]×2.5[b]=0.23	0.20[a]×4.64[c]=0.93	3.27	1.87
0.1Pd/Z12-E	0.76[a]	0.10[a]×2.5[b]=0.25	0.14[a]×4.63[c]=0.65	3.26	1.66
0.3Pd/Z12-E	0.80[a]	0.10[a]×2.5[b]=0.25	0.10[a]×4.26[c]=0.43	2.52	1.48

[a] Wt.% of mono-branched (M), multi-branched (B) *iso*-hexadecanes and cracked products (C).

[b] Acid steps number involved in the transformation of one molecule of *n*-C_{16} into B product.

[c] Acid steps number involved in the transformation of one molecule of *n*-C_{16} into C product.

[d] N_C value was the number of formed molecules produced by one cracked *n*-hexadecane molecule.

[e] $n_{as}=M\times1+B\times2.5+C\times[4+(Nc-2)/2]$

The n_{as} value represents the average number of acid sites of one *n*-hexadecane molecule contacted during the hydroisomerization reaction between two adjacent metal sites. The n_{as} value was calculated based on the reaction results at *n*-hexadecane conversion of ~20 % (in the dynamic

control range) by employing the above equation [1, 2]. (SI)

Comment: (3) Should be clarify more the synergetic effects of the larger ratio of metal to acid sites improved the catalytic selectivity for *n*-hexadecane hydroisomerization when bifunctional catalyst has been prepared by the glow discharge plasma reduction method?

Author reply:

Response: Thanks a lot for the comment. We gladly to accept this suggestion, and clarified more the synergetic effects of the larger ratio of metal to acid sites (C_{Pd}/C_{H+}) improved the catalytic selectivity for *n*-hexadecane hydroisomerization when *x*Pd/Z12-E bifunctional catalysts has been prepared by the glow discharge plasma reduction method.

Action: In the manuscript, we have added the following:

"For the *x*Pd/Z12-E series of catalysts, the *iso*-hexadecane yield is also significantly improved when Pd loading increases from 0.1 wt.% to 0.3 wt.%, as well as the C_{Pd}/C_{H+} ratio correspondingly increases from 0.053 to 0.345. The *x*Pd/Z12-E series of catalysts present obviously higher maximum *iso*-hexadecane yield than that of *x*Pd/Z12-C catalysts with same Pd loading at conversion of ~95%, which can be explained by the following reasons. First, *x*Pd/Z12-E catalysts have larger Pd sites density and C_{Pd}/C_{H+} ratio, which is 1.7~2.1 times more than that of *x*Pd/Z12-C series of catalysts with the same Pd loading, which will facilitate hydrogenation of *iso*-alkene intermediates to *iso*-hexadecane rather than further cracking into light hydrocarbons. Furthermore, *x*Pd/Z12-E catalysts expose more Pd (111) facets because of the kinetically controlled growth mechanism for the Pd nanoparticles, which leads to a much stronger H_2 chemical adsorption and dissociation capacity compared with *x*Pd/Z12-C series catalysts with exposure of more Pd (100) facets [58]." (Page 24 line 15 - Page 25 line 6)

Comment: (4) Conclusion should be re-written.

Author reply:

Response: Thanks a lot for the comment. We accepted the reviewer's suggestion and have re-written the conclusion.

Action: We have re-written the conclusion, the content is as follows:

*x*Pd/Z12-E Bifunctional catalysts with 0.1 wt.% and 0.3 wt.% Pd loaded on nanosized ZSM-12 zeolite are prepared by novel in-situ glow discharge plasma reduction method at room temperature. Compared with *x*Pd/Z12-C catalysts with the same Pd loadings prepared by the conventional hydrogenation reduction method, *x*Pd/Z12-E catalysts present higher Pd dispersion and more exposed Pd (111) facets.

Based on the research results of catalytic performance for the *n*-hexadecane hydroisomerization obtained at different temperature ranges, we find that the density of Pd active sites and hydrogen activation ability have more significant influences to the catalystic activity than that of the acidity at higher reaction temperature (in the thermodynamically controlled range). Moreover, the stronger hydrogen activation ability caused by more exposed Pd (111) facets is more important compared with the larger ratio of metal to acid sites (C_{Pd}/C_{H+}) for the improvement of the catalytic performance. Accordingly, the maximum yield of *iso*-hexadecane achieved over the 0.1Pd/Z12-E catalyst with 0.1 wt.% Pd loading ($C_{Pd}/C_{H+} = 0.053$) is close to that obtained over the 0.3Pd/Z12-C catalyst with three times the Pd loading ($C_{Pd}/C_{H+} = 0.161$). Furthermore, *x*Pd/Z12-E series of catalysts show higher yield of *iso*-hexadecane and selectivity for multi-branched isomers, as well as excellent catalytic stability, due to the stronger hydrogen activation ability and favourable

metal-acid balance. The maximum *iso*-hexadecane yield of 80.2 % and selectivity for multi-branched *iso*-hexadecane of 53.8 % at *n*-hexadecane conversion of 93.6 % was obtained over the 0.3Pd/Z12-E catalyst.

Therefore, the in-situ glow discharge plasma reduction is an effective method to prepare highly effective bifunctional catalysts with a low noble metal loading and excellent catalytic performance for the hydroisomerization of long-chain *n*-alkanes, which show a further industrial application potential for production of second generation biodiesel with outstanding low-temperature fluidity. (Page 29 line 9- Page 31 line 2)

Comment: (5) Should be corrected some typographical errors.

Author reply:

Response: Thanks very much for the comment. We found some typographical errors and made corrections.

Action: We have revised the typographical errors in the manuscript and highlighted the changes in RED.

Reviewer #2:

Comment: (1) In the introduction, there is no specific research goal. As it stands, the introduction suggests the hydroisomerization of n-alkanes to MoB-iC16 (used as fuel components), and the article focuses on MuB-iC16 (fuel oil and lubricating oil components). The introduction needs to be slightly edited and the literature enriched.

Author reply:

Response: Thanks very much for this constructive comment. We have revised the last paragraph of the Introduction section, in which we clearly stated the purpose of our research: it is to establish a new method for the preparation of high-efficiency zeolite-based bifunctional catalysts *x*Pd/Z12-E series of catalysts with low noble metal loadings and high hydrogen activation ability for the hydroisomerization of *n*-paraffins, and to elucidate their structure-performance relationships and clarify the reasons for of the higher *iso*-hexadecane yield and selectivity to multi-branched isomers.

Action: We accepted the reviewers' suggestions and refined the last paragraph of the Introduction, and we enriched literature (newly added reference 4, 6, 10, 11, 24, 27, 33 and 35, the serial numbers of other reference are successively followed) . The revised last paragraph of the Introduction section is as follows:

"In this paper, we aim to establish a new method for the preparation of high-efficiency zeolite-based *x*Pd/Z12-E bifunctional catalysts on the nanosized ZSM-12 zeolite with low noble metal loadings (0.1 wt.% and 0.3 wt.% Pd) for the hydroisomerization of *n*-hexadecane. The structure-performance relationships of prepared bifunctional catalysts are elucidated and the reasons for the highest *iso*-hexadecane yield of 80.2 % and selectivity for multi-branched isomers of 53.8 % over the 0.3Pd/Z12-E catalyst at *n*-hexadecane conversion of 93.6 % are also discussed. Different from the works reported by other scholars, we employ a novel in-situ room temperature electron reduction method to load Pd with higher dispersion and stronger ability to activate hydrogen than *x*Pd/Z12-C catalysts prepared by the traditional hydrogen thermal reduction method. Moreover, the synthesized nano-ZSM-12 zeolite with larger openings size and abundant intergranular mesopores formed by the accumulation of small grains with an average size of

approximately 40-50 nm is used as an acidic support, which can effectively improve the diffusion properties of *iso*-olefin intermediates and inhibit their cracking. With above modifications, more multi-branched *iso*-hexadecane in the *n*-hexadecane hydroisomerization products at the maximum yield are obtained, which have excellent low temperature flow properties as a second generation biodiesel component." (Page 6 line 7 - Page 7 line 2)

Comment: (2) Change the citation method. Author et al. [x]. Examples page 7 line 60, page 9 line 24.

Author reply:

Response: Thanks very much for the comment. It is really our oversight. We have modified the corresponding citation method.

Action: We changed the citation method to "Author et al. [x]", and highlighted the changes in bright yellow.

The modified content is as follows:

Zschiesche *et al.* [25] compared the catalytic performance of C_{10}-C_{13} *n*-alkanes hydroisomerization over platinum-containing zeolite bifunctional catalysts with different one- and three-dimensional 10-（ZSM-5, ZSM-22, ZSM-23）and 12-membered-ring (Beta, HM and ZSM-12) pores. (Page 3 line 18-22)

Li *et al.* [40] prepared Pd/ZSM-22 catalysts via this method and found that the prepared catalysts demonstrate higher Pd dispersion, more favourable metal-acid balance and improved catalytic performance for *n*-hexane hydroisomerization. (Page 5 line 21 - Page 6 line 2)

Comment: (3) Table 2 - perhaps it would be worth determining the effect of the synthesis method on the distribution of Lewis and Brønsted acid sites in catalysts. Report the Pd particle sizes determined by the chemisorption method.

At what temperature are the results shown in Fig. 6 b, c, d? Which is a common comparative parameter? In their present form, the drawings unable the interpretation of the results.

Author reply:

Response: Thanks very much for the valuable comment. We accepted the reviewer's suggestion to supplement the manuscript with data of Lewis acid sites, distribution of Brønsted and Lewis acid sites, and Pd particle sizes measured by chemisorption, and discussed the regularity of the supplemented data.

The data in Fig. 6 b, c, d were obtained over four catalysts at *n*-hexadecane conversion of approximately 95 % (95.9% at 310 ºC, 94.3% at 300 ºC, 95.7% at 300 ºC and 93.6% at 305 ºC over 0.1Pd/Z12-C, 0.3Pd/Z12-C, 0.1Pd/Z12-E and 0.3Pd/Z12-E, respectively). We have added this explanation to the title of the Fig. 6.

For the hydroisomerization reaction of *n*-alkane, the common main comparative parameters for evaluating the catalytic performance are the conversion of *n*-alkane, the selectivity and yield of *iso*-hexadecane. We chose the result when the conversion of *n*-hexadecane is close to 95% to establish the relationship between the yield of *iso*-hexadecane and C_{H+} and C_{Pd}/C_{H+} ratio, reapectively (corresponding to Fig. 6b, 6c), based on the following two considerations:

1. Comparing yields of *iso*-hexadecane is also equivalent to comparing selectivity for

iso-hexadecane at the same conversion of *n*-hexadecane. Therefore, the three most important evaluation parameters of catalytic performance are given in the Fig. 6b, 6c. In these figures, we reveal the effect of C_{H+} and C_{Pd}/C_{H+} ratio on the yield of *iso*-hexadecane over different catalysts.

2. The maximum yield of *iso*-hexadecane obtained over these four catalysts is also under the condition that the conversion of *n*-hexadecane is close to 95%. Therefore, the experimental results obtained under this condition can not only reveal the scientific laws of the influence of different preparation methods on the catalytic performance, but also have important value for the development of catalysts, which can be used to produce green biodiesel with excellent low temperature fluidity.

Action:

1. We supplement the data of Lewis acid sites, distribution of Brønsted acid sites in the Table S1, and add data of Pd particle sizes measured by chemisorption in Table 2, and explained the related result. (Page 13 line 12-16; Page 14 line 9-11)

Table 2. The Brønsted acid density and metal characteristics of ZSM-12 zeolite and all Pd/Z12 catalysts.

Sample	Brønsted acid sites ($\mu mol\ g^{-1}$)		D_{Pd} (%)[a]	C_{Pd} ($\mu mol\ g^{-1}$)[b]	C_{Pd}/C_{H+}[c]	Pd size (nm)[d]
	Strong	Total				
ZSM-12	23.5	27.3	-	-	-	-
0.1Pd/Z12-C	22.0	26.2	8.9	0.84	0.032	12.5
0.3Pd/Z12-C	20.5	25.1	14.3	4.03	0.161	7.8
0.1Pd/Z12-E	21.1	25.4	14.4	1.35	0.053	7.8
0.3Pd/Z12-E	18.1	23.3	28.5	8.03	0.345	3.9

[a] Determined by H_2 chemisorption, [b] Calculated by Pd dispersion, [c] Calculated by total Brønsted acid sites, [d] Determined by the chemisorption method.

Table S1 supplemented to the SI section is as follows:

Table S1 The acid sites density of ZSM-12 zeolite and all Pd/Z12 catalysts.

Sample	BAS[a] (C_{H+}, $\mu mol\ g^{-1}$)	LAS[b] ($\mu mol\ g^{-1}$)	TAS[c] ($\mu mol\ g^{-1}$)	BAS Distribution[d] (%)
ZSM-12	23.5	27.3	50.8	56.3
0.1Pd/Z12-C	22.0	26.2	48.2	59.3
0.3Pd/Z12-C	20.5	25.1	45.6	49.9
0.1Pd/Z12-E	21.1	25.4	46.5	53.9
0.3Pd/Z12-E	18.1	23.3	41.4	49.7

[a] Brønsted acid sites, [b] Lewis acid sites, [c] Total acid sites, [d] Distribution of Brønsted acid sites in the total acid sites.

2. Combined with the reviewer's comment (4), we supplemented the content of Figure 6, and clarified the conditions for obtaining the yield on the revised title of figure 6 (at conversion of about 95%). These revisions and explanations are clarified together in the action for answer to reviewer's comment (4).

Comment: (4) Fig. 6d, comparing the distribution of products at a conversion of about 95% is not correct. It is better to compare the distribution of products with a conversion of approx. 50%, then products that are formed as a result of secondary reactions are avoided. Please change it or show the sense of such a catalyst comparison.

Author reply:

Response: Thanks very much for the comment. Based on the reviewers' suggestions, we also analyzed the distribution of mono-branched, multi-branched *iso*-hexadecane and cracking products at *n*-hexadecane conversion of approx. 50 % and approx. 20%, and supplemented the results to revised Fig. 6.

It should be noted that, we wish to keep the results of the products distribution at a conversion of about 95% in Fig 6 in the manuscript, and the reasons are as follows: On the one hand, the secondary cracking reactions at conversion of approx. 95 % are suppressed compared with result obtained at conversion of approx. 50% (revised Fig. S8). On the other hand, the maximum yield of *iso*-hexadecane and highest selectivity to multi-branched isomers, which has a lower freezing point as a green biodiesel component, are also obtained over all catalysts at the *n*-hexadecane conversion of about 95%, and the products distribution shows a good structure-performance relationship at this conversion. Therefore, comparing the distribution of products at a conversion of about 95% (thermodynamic control range) can not only reveal the influence laws of preparation methods of the bifunctional catalysts to the catalytic performance, but also have important value for the development of industrial catalysts promising for production of green biodiesel with excellent low temperature fluidity.

Action: We supplemented the results of distribution of mono-branched, multi-branched *iso*-hexadecane and cracking products at *n*-hexadecane conversion of approx. 50 % to revised Figure 6e along with results for conversion of approx. 20 % (Figure 6d) , and kept the results of the products distribution at a conversion of about 95 % in revised Figure 6f of the manuscript. We also added the graph showing performance changes of MoB-C_{16}, MuB-C_{16} and cracked products on conversion as the current Figure S7, and the original Figure S7 was changed to Figure S9. The fraction of cracking products at conversion of about 20 %, 50 % and 95 % was shown in revised Figure S8, and we added the interpret about results of revised Figure 6 and Figure S8.
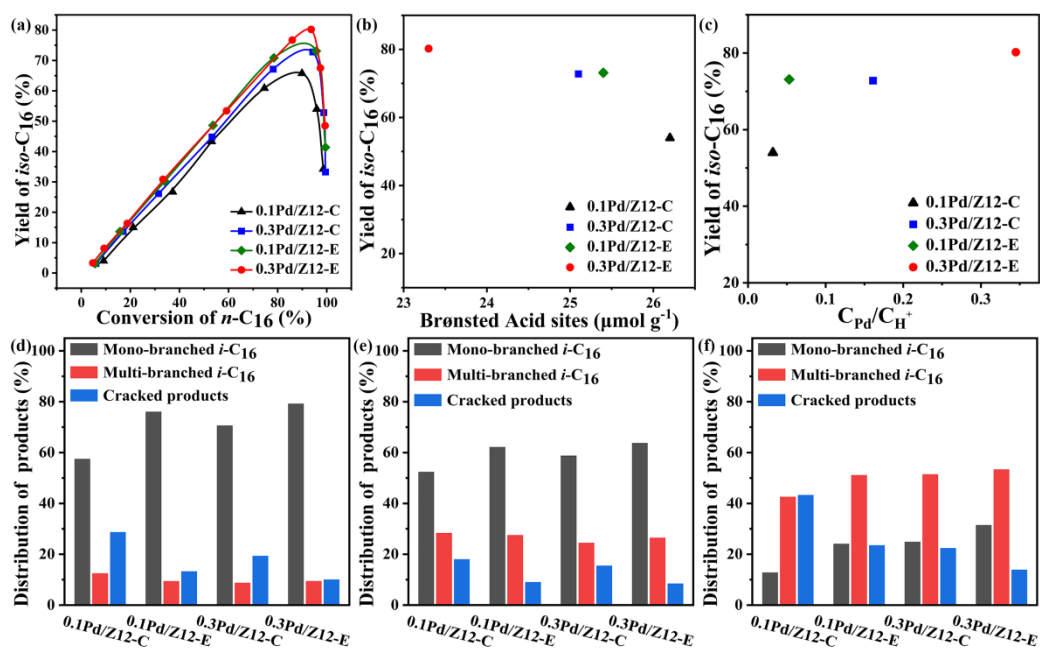
The revised Figure 6 is as follows:

Figure 6. The relationships between *iso*-hexadecane yield and *n*-hexadecane conversion (a); *iso*-hexadecane yield *vs* C_{H+} (b) and C_{Pd}/C_{H+} ratio (c) at *n*-hexadecane conversion of ~ 95 %; and the distribution of products over different catalysts at *n*-hexadecane conversion of ~ 20 % (d), ~ 50 % (e) and ~ 95% (f).

The supplementary and refined explanation of revised Figure 6 is as follows:

"In addition to the catalytic activity, the selectivity for branched isomers, and products distribution are more important evaluation parameters of the bifunctional catalysts for the hydroisomerization of long-chain *n*-alkanes, especially for multi-branched isomers, which are expected to be used as green biodiesel component with excellent low temperature fluidity. Therfore, the relationships between *iso*-hexadecane yield and conversion, C_{H+} and C_{Pd}/C_{H+} ratio are investigated to further discuss the impact factors of *iso*-hexadecane yield over two series of catalysts at *n*-hexadecane conversion ~ 95 % (in the thermodynamically controlled range, in which more multi-branched isomers will be generated). Simultaneously, the products distribution at representative conversions (~ 20 %, ~ 50% and ~ 95 %) are also compared and the results were shown in Figure 6." (Page 22 line 8-18)

From Figure 6a, although the 0.3Pd/Z12-E catalyst has the lowest activity among all catalysts at the same tempereture, there is no significant difference in *iso*-hexadecane yield when the *n*-hexadecane conversion is lower than ~20 % (in dynamic controlled range), except for the 0.1Pd/Z12-C catalyst with minimum matal sites density. The low *iso*-hexadecane yield over the 0.1Pd/Z12-C catalyst can be explained by its maximum n_{as} value of 2.28, which represents the average number of acid sites of one *n*-hexadecane molecule contacted during the hydroisomerization reaction between two adjacent metal sites, calculated based on the reaction results at *n*-hexadecane conversion of ~20 % (Table S2). It is found that the n_{as} value of the 0.1Pd/Z12-C catalyst is greater than that of 0.3Pd/Z12-C (1.87), 0.1Pd/Z12-E (1.66) and 0.3Pd/Z12-E (1.48), indicating that stronger cracking reactions even appeared at lower temperatures (corresponding conversion is less than ~20 %) when the metal sites are severely deficient. It is worth noting that, there is a greater difference in the *iso*-hexadecane yield over two

series of catalysts in thermodynamic controlled range (at n-hexadecane conversion of 80~95 %). Figure 6b, 6c present that the reduced C_{H+} and increased C_{Pd}/C_{H+} ratio are both beneficial for improving the *iso*-hexadecane yield. For the 0.1Pd/Z12-C catalyst with highest Brønsted acid density and lowest C_{Pd}/C_{H+} ratio, the maximum *iso*-hexadecane yield is only 65.8 % at n-hexadecane conversion of 89.9 % due to the lack of metal sites and weak hydrogenation function, resulting in strong cracking of isomeric alkene intermediates on the Brønsted acid sites. While for the 0.3Pd/Z12-C catalyst, the metal function is effectively improved because of the increase of Pd loading from 0.1 wt.% to 0.3 wt.%, as well as the Pd dispersion (from 8.9 % to 14.3 %) and the C_{Pd}/C_{H+} ratio (from 0.027 to 0.161). Accordingly, an increased *iso*-hexadecane yield of 72.8 % is achieved over the 0.3Pd/Z12-C catalyst at n-hexadecane conversion of 94.3 %. For the xPd/Z12-E series of catalysts, the *iso*-hexadecane yield is also significantly improved when Pd loading increases from 0.1 wt.% to 0.3 wt.%, as well as the C_{Pd}/C_{H+} ratio correspondingly increases from 0.053 to 0.345. The xPd/Z12-E series of catalysts present obviously higher maximum *iso*-hexadecane yield than that of xPd/Z12-C catalysts with same Pd loading at conversion of ~95%, which can be explained by the following reasons. First, xPd/Z12-E catalysts have larger Pd sites density and C_{Pd}/C_{H+} ratio, which is 1.7~2.1 times more than that of xPd/Z12-C series of catalysts with the same Pd loading, which will facilitate hydrogenation of *iso*-alkene intermediates to *iso*-hexadecane rather than further cracking into light hydrocarbons. Furthermore, xPd/Z12-E catalysts expose more Pd (111) facets because of the kinetically controlled growth mechanism for the Pd nanoparticles, which leads to a much stronger H_2 chemical adsorption and dissociation capacity compared with xPd/Z12-C series catalysts with exposure of more Pd (100) facets [58]. (Page 23 line 1 - Page 25 line 6)

In order to clarify the change of catalytic performance at different n-hexadecane conversion, the distribution of mono-branched, multi-branched *iso*-hexadecanes and cracked products over all catalysts are compared at conversion of ~20 %, ~50 % and ~95 %, respectively, and the results are shown in Figure 6 and Figure S7, S8. It is found that, for each series of catalysts, the higher selectivity of mono-branched isomers and less cracked products are achieved over the catalysts with more Pd loading due to the greater metal active sites density and C_{Pd}/C_{H+} ratio. The mono-branched *iso*-hexadecanes are mainly products over all catalysts at ~20 % and ~50 % conversion. However, the selectivity of mono-branched isomers tends to decrease with increase of conversion, and multi-branched isomers enhanced accordingly. When the n-hexadecane conversion reach to about 95 %, the selectivity for multi-branched *iso*-hexadecane over all catalysts are maximum, which is about 2 times higher than that of mono-branched isomers. This result can be attributed to the improvement of diffusion properties of multi-branched *iso*-alkene intermediates because of abundant intergranular mesopores formed by the accumulation of ZSM-12 zeolite nanoparticle and the hence inhibition of its further cracking. In addition, the selectivity for cracked products at conversion of ~95 % is highest for each catalysts due to the intensify cracking of *iso*-olefin intermediate at corresponding higher temperatures. The xPd/Z12-E catalysts demonstrate higher selectivity for both mono-branched and multi-branched *iso*-hexadecane, and lower selectivity for craking products than those of the xPd/Z12-C catalysts with the same Pd loading at a similar conversion, which can be originated from the promoted hydrogenation of branched *iso*-alkene intermediates to form *iso*-hexadecane on Pd active sites caused by the enhanced metal function and synergistic catalysis of metal-acid sites [44]. (Page 25 line 20 - Page 26 line 21)

We list the cracked products at conversion of ~20 % ~50 % and ~95 %, respectively, in the revised Fig. S8, and added the following explanation: "The law of cracked products distribution is the same at different conversion over all catalysts, and the distribution of the C_3-C_6 light hydrocarbon as well as the C_4/C_{12} and C_5/C_{11} values obtained at n-hexadecane conversion ~95% over the four catalysts decreases in the order of 0.1Pd/Z12-C > 0.3Pd/Z12-C > 0.1Pd/Z12-E > 0.3Pd/Z12-E (shown in Fig. S8 and Tab. S4), suggesting that the secondary cracking is reduced over the xPd/Z12-E catalysts due to the enhanced metal function and synergistic catalysis between the metal sites and acid sites." (Page 26 line 21 - Page 27 line 6)

The revised Figure S8 is as follows:
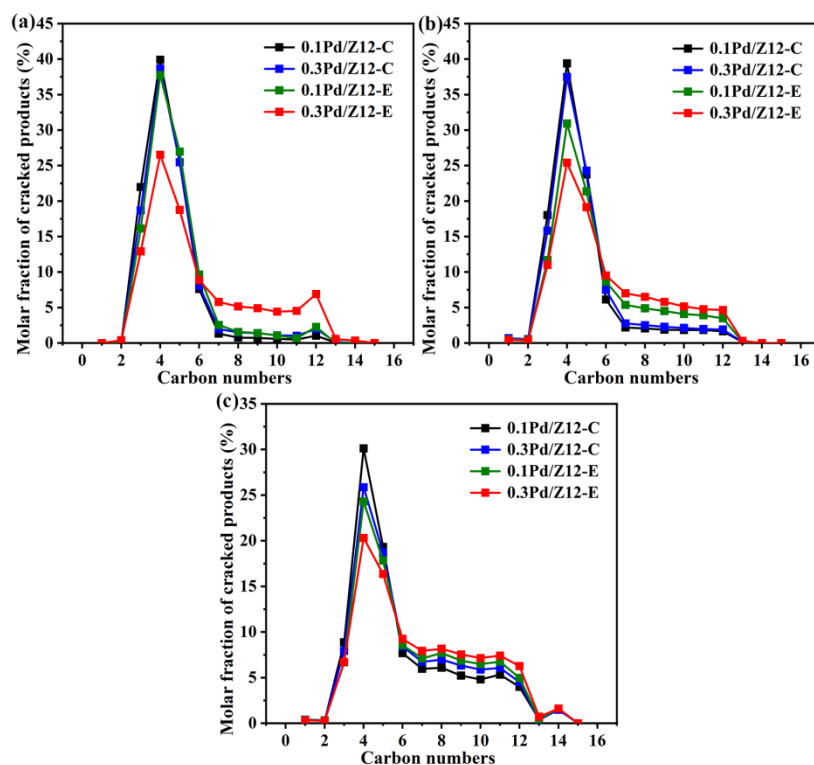
Figure S8. The distribution of cracking products (mol.%): percentage of cracked products as a function of the number of their carbon atoms over all catalysts at n-hexadecane conversion of about 20 % (a), 50 % (b) and 95 % (c)

Comment: (5) The share of MoB isomerization products is small when compared to all isomerization and cracking products. Please add graphs showing performance changes of MoBC16, MuBC16 and cracked products on one chart depending on temperature or conversion.
Author reply:
Response: Thanks very much for this valuable comment. As the reviewer pointed out, the proportion of MoB isomerization products varies greatly at different conversion, and the mono-branched iso-hexadecanes are mainly products over all catalysts at ~20 % and ~50 % conversion. However, the selectivity of mono-branched isomers tends to decrease with increase of conversion from 20% to 95%, and the selectivity for multi-branched isomers enhanced accordingly. We have clarified this point in response to reviewer's comment (4) and the corresponding action section, and added the results and discuss of product distribution at

conversion of ~20 %, ~50 %, and ~95% (correspond to the dynamics controlled range, the intermediate stage and the thermodynamic controlled range, respectively) to Figure 6d-6f of the revised manuscript. We accepted reviewer's comment, however, considering the limitations of manuscript length and in order to avoid duplicate information in the manuscript, we added the graphs showing performance changes of $MoBC_{16}$, $MuBC_{16}$ and cracked products on one chart depending on conversion to support information section.

Action: We add the graphs showing performance changes of $MoBC_{16}$, $MuBC_{16}$ and cracked products on one chart depending on conversion to support information section as Figure S7 of the revised manuscript, and the original Figure S7 was changed to Figure S9. To avoid repetitive discussions the obtained rules, Figure S7 are discussed together with the results presented in revised Figure 6. (Page 25 line 20 - Page 26 line 21)
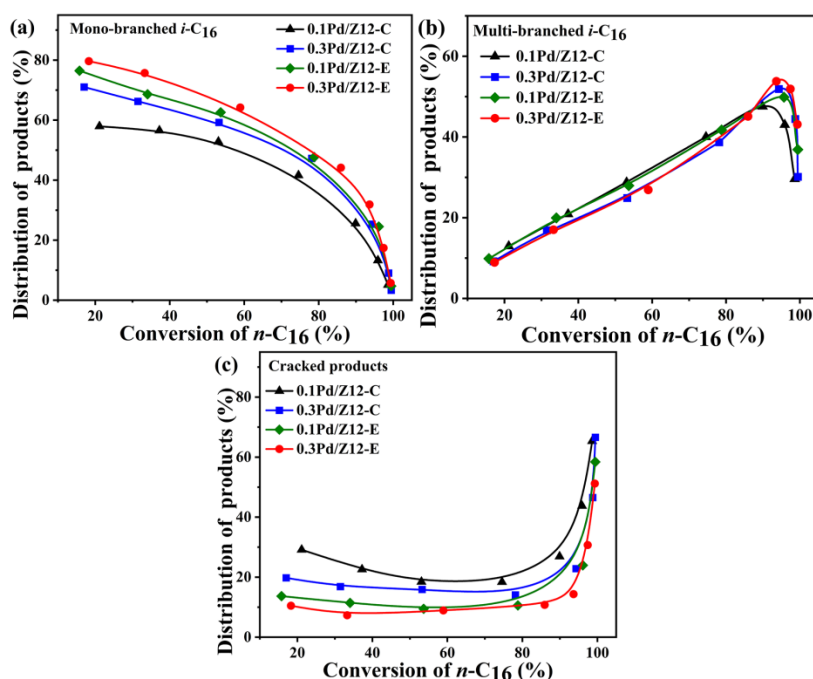
Figure S7. The relationships between distribution of products and conversion: mono-branched
i-C_{16} (a), multi-branched i-C_{16} (b) and cracked products (c)

Comment: (6) Fig. S7 the differences between the catalysts are very small, so what is the positive effect of the new method of applying Pd to the support?

Author reply:

Response: Thanks a lot for the comment. Exactly as the reviewer pointed out, in Fig. S7 (in the revised manuscript, the Figure S7 was changed to Figure S9 due to the addition of two new figures before it), the differences in products distribution of mono-branched *iso*-hexadecanes between the catalysts are very small. This is because the reaction mechanism of n-alkanes hydroisomerization ("key-lock" mechanism or "pore mouth" mechanism) is mainly determined by the textural properties of the molecular sieves that provide the acid sites of the bifunctional catalyst. All catalysts studied in this manuscript were prepared by using nano-ZSM-12 zeolite as the acidic support. The larger opening pore size of nano-ZSM-12 zeolite (opening diameter of 0.56×0.62 nm) is slightly larger than the dynamic diameter of the mono-branched isomers, which allows the

n-hexadecane molecules to diffuse deep into the micropore channels to be isomerized and diffuse out of the pore channels fast to generate more 3-methyl- ~ 8-methylpentadecane products with a centrally located branch. Therefore, the hydroisomerization of *n*-hexadecane over all catalysts based on nano-ZSM-12 follows the "key-lock" mechanism. The very small differences between the catalysts only appeared in distribution of mono-branched *iso*-hexadecane. In addition, we are currently working on the isomorphic replacement modification of nano-ZSM-12 zeolite to prepare [Ga, Al]ZSM-12 zeolites with hierarchical pore structure, and the bifunctional catalysts prepared on these modified zeolites as acidic support exhibit interesting results in hydroisomerization reactions that differ from microporous ZSM-12 zeolites based catalysts, which will be reported in future work.

The positive effect of the new method is as follows：1. The new method of in-situ glow discharge plasma reduction at room temperature to prepare xPd/Z12-E bifunctional catalysts with lower Pd loading (0.1wt.% and 0.3wt.% Pd) present higher Pd dispersion (the Pd active sites density on the xPd/Z12-E catalysts is 1.6~2.0 times that on xPd/Z12-C catalysts) and more exposed Pd (111) facet with stronger hydrogen activation ability compared with xPd/Z12-C catalysts with the same Pd loading prepared by the conventional hydrogenation reduction method. These modifications can promote the hydrogenation of isomeric intermediates to inhibit the cracking reaction and thereby improve the catalytic performance over xPd/Z12-E catalysts.

2. The maximum yield of *iso*-hexadecane at similar *n*-hexadecane conversion (~95 %) over the xPd/Z12-E bifunctional catalysts is also greatly improved than that of the xPd/Z12-C catalysts with the same Pd loading. The maximum yields of *iso*-hexadecane over the 0.1Pd/Z12-C and 0.1Pd/Z12-E catalysts are 65.7 % and 73.1 %, respectively. The maximum yields of *iso*-hexadecane over the 0.3Pd/Z12-C and 0.3Pd/Z12-E catalysts with 0.3wt.% Pd loading increased to 72.8 % and 80.2 %, respectively.

3. The maximum yield of *iso*-hexadecane achieved over the 0.1Pd/Z12-E catalyst with 0.1 wt.% Pd loading ($C_{Pd}/C_{H+} = 0.053$) is close to that obtained over the 0.3Pd/Z12-C catalyst with three times the Pd loading ($C_{Pd}/C_{H+} = 0.161$). Based on this result, we proved the following conclusions "stronger hydrogen activation ability caused by more exposed Pd (111) facets is more important than larger ratio of metal to acid sites (C_{Pd}/C_{H+}) for the improving the catalytic performance".

4. TG analysis of the catalyst after 100 h time on stream showed that the employment of glow discharge plasma reduction was beneficial for the inhibition of carbon deposition and Pd aggregation on the bifunctional catalysts to maintain outstanding catalytic stability.

Action: In order to more clearly illustrate the results expressed in Figure 7 (In the revised manuscript, the Figure S7 was changed to Figure S9), we have revised the relevant text, and the revised content is as follows:

"From the product distribution of mono-branched *iso*-hexadecane over two series of catalysts (Fig. S9), it can be seen that the distribution law for all catalysts is similar, and the proportion of 2-methylpentadecane is much less than that of mono-branched *iso*-hexadecanes with a centrally located branch. This result is attributed to the fact that the reaction mechanism of *n*-alkanes hydroisomerization is mainly determined by the textural properties of the molecular sieves that provide the acid sites of the bifunctional catalysts. All catalysts are prepared by using nano-ZSM-12 zeolite as the acidic support. The larger pore size of nano-ZSM-12 zeolite (opening diameter of 0.56 × 0.62 nm) is slightly larger than the dynamic diameter of the mono-branched

isomers, which allows the *n*-hexadecane molecules to diffuse deep into the micropore channels to be isomerized and diffuse out of the pore channels fast to generate more 3-methyl- ~ 8-methylpentadecane products with a centrally located branch. Therefore, the hydroisomerization of *n*-hexadecane over all catalysts based on nano-ZSM-12 zeolite follows the "key-lock" mechanism." (Page 27 line 7 - Page 27 line 20)

Comment: (7) "Moreover, the distribution of the C_3-C_6 light hydrocarbon as well as the C_4/C_{12} and C_5/C_{11} values obtained at *n*-hexadecane conversion ~95% over the four catalysts decreases in the order of 0.1Pd/Z12-C > 0.3Pd/Z12-C > 0.1Pd/Z12-E >0.3Pd/Z12-E (shown in Fig. S8 and Tab. S2), suggesting that secondary cracking is effectively inhibited due to the enhanced metal function of the *x*Pd/Z12-E catalysts." This sentence is not true! From Fig S8 it can be seen, that C_4 is the main product of cracking, which proves that secondary cracking is taking place to a very large extent. Please rewrite this paragraph.

Author reply:

Response: Thanks a lot for the comment. We agreed with the reviewer's suggestion. Indeed, C_4 is the main product of cracking, which proves that secondary cracking generated to varying degrees over different catalysts (in revised Fig. S8). In the sentence "suggesting that secondary cracking is effectively inhibited due to the enhanced metal function of the *x*Pd/Z12-E catalysts", what we wanted to say was that the secondary cracking degree was relatively low (secondary cracking is effectively inhibited) over the *x*Pd/Z12-E catalysts than that over the xPd/Z12-C catalysts. But as the reviewer pointed out, the secondary cracking reaction could not be avoided for hydroisomerization of long-chain *n*-alkanes.

Action: Based on the reviewer's suggestion, we rewrote this paragraph reflected the revised Figure S8, it is as follows:

"The law of cracked products distribution is the same at different conversion over all catalysts, and the distribution of the C_3-C_6 light hydrocarbon as well as the C_4/C_{12} and C_5/C_{11} values obtained at *n*-hexadecane conversion ~95% over the four catalysts decreases in the order of 0.1Pd/Z12-C > 0.3Pd/Z12-C > 0.1Pd/Z12-E > 0.3Pd/Z12-E (shown in Fig. S8 and Tab. S4), suggesting that the secondary cracking is reduced over the *x*Pd/Z12-E catalysts due to the enhanced metal function and synergistic catalysis between the metal sites and acid sites." (Page 26 line 21 - Page 27 line 6)

Reference for Response

1. Wang Y, Tao Z, Wu B, Xu J, Huo C, Li K, et al. Effect of metal precursors on the performance of Pt/ZSM-22 catalysts for *n*-hexadecane hydroisomerization. J Catal 2015;322:1-13.

2. Liu S, Ren J, Zhu S, Zhang H, Lv E, Xu j, et al. Synthesis and characterization of the Fe-substituted ZSM-22 zeolite catalyst with high *n*-dodecane isomerization performance. J Catal 2015;330:485-496.

The effective xPd/Z12-E bifunctional catalysts are prepared by in-situ glow-discharge plasma reduction.

Pd nanoparticles in xPd/Z12-E have higher Pd dispersion, as well as more Pd (111) facets.

The synergistic effect of the larger C_{Pd}/C_{H+} ratio and the stronger metal function enhanced catalytic performance.

ZSM-12 with 12-ring pore structure is conducive to the formation of multi-branched isomers.

xPd/Z12-E catalysts show higher iso-hexadecane yield and excellent catalytic stability in the n-hexadecane hydroisomerization.

Highly effective Pd/ZSM-12 bifunctional catalysts by in-situ glow discharge plasma reduction: the effect of metal function on the catalytic performance for *n*-hexadecane hydroisomerization

Hailong Lin[a]*, Wei Wang*[a,*]*, Oleg V. Kikhtyanin*[b]*, David Kubicka*[b]*, Zhaolu Feng*[a]*,*

Chunmu Guo[a]*, Xuefeng Bai*[a]*, Linfei Xiao*[a] *and Wei Wu*[a,*]

[*] Corresponding authors
E-mail addresses: 2016053@hlju.edu.cn (W. Wang), wuwei@hlju.edu.cn (W. Wu).

[a] National Center for International Research on Catalytic technology, Key Laboratory of Functional Inorganic Materials Chemistry (Ministry of Education), Key Laboratory of Chemical Engineering Process ＆ Technology for High-Efficiency Conversion, College of Heilongjiang Province, School of Chemistry and Material Sciences, Heilongjiang University, Harbin 150080, Heilongjiang, China.

[b] University of Chemistry and Technology Prague, Department of Petroleum Technology and Alternative Fuels, Technická 5, 166 28 Prague, Czech Republic

Abstract: *Background:* Although the zeolite-based bifunctional catalysts loaded noble metal have higher catalytic activity, it is still a great challenge to reduce the noble metal loading while maintaining the high selectivity for branched isomers in the long-chain *n*-alkane hydroisomerization.

Methods: A novel method of in-situ glow discharge plasma reduction at room temperature is introduced to prepare the highly effective bifunctional catalysts (*x*Pd/Z12-E) with 0.1 wt.% and 0.3 wt.% Pd loaded on nanosized ZSM-12 zeolite for *n*-hexadecane hydroisomerization. For comparison, *x*Pd/Z12-C catalysts with the

same Pd loadings were prepared by the conventional hydrogenation reduction method.

Significant Findings: The maximum yield of *iso*-hexadecane achieved over the *x*Pd/Z12-E catalyst is much higher than that of *x*Pd/Z12-C catalysts, which is originated from the synergetic effects of the larger ratio of metal to acid sites and improved hydrogen activation ability caused by more exposed Pd (111) facets. Besides, the 0.1Pd/Z12-E catalyst exhibits excellent catalytic stability. Our work provides a effective pathway for the development of bifunctional catalysts for production of clean biodiesel with outstanding low-temperature fluidity.

Keywords. Nanosized ZSM-12 zeolite; Pd nanoparticle; Bifunctional catalyst; Glow discharge plasma reduction; Hydroisomerization

1. Introduction

Currently, the development of green fuels has captured considerable attention because of decreasing traditional fossil resources and serious problems of environmental pollution was employed, respectively [1-3]. For this purpose, biodiesel produced from abundant bio-oil has proven to be a renewable and clean fuel since it is free of nitrides, sulphides, olefins and aromatics [4]. Furthermore, compared with the first-generation biodiesel with fatty acid methyl ester (FAME) as the main component, the second-generation biodiesel based on *iso*-alkanes indicates great potential for employment as an alternative energy source due to its ideal miscibility with fossil diesel in any proportion and excellent low-temperature fluidity [5,6].

The second-generation biodiesel is generally produced by the formation of C_{15}~C_{18} *n*-alkanes via the hydrodeoxygenation of bio-oils and their further hydroisomerization to obtain *iso*-alkanes [7-9]. However, because the hydroisomerization is inevitably accompanied by cracking reaction, the yield of long-chain *iso*-alkanes is usually unsatisfactory [10,11]. Therefore, design and preparation of highly effective catalysts composed of metal sites and Brønsted acid sites are effective methods to increase the yield of *iso*-alkanes [12-14]. During the hydroisomerization process, metal sites catalyse the (de)hydrogenation of hydrocarbons, while Brønsted acid sites catalyse skeletal isomerization and further cracking [15-17]. Accordingly, the favourable metal-acid balance is one of the crucial factors required to improve the catalytic performance of bifunctional catalysts [18,19].

The Brønsted acid sites are generally provided by zeolite and silicoaluminophosphate molecular sieves. It has been proven that the *iso*-alkanes yield over zeolites with one-dimensional microporous structures (e.g., mordenite zeolite, ZSM-12 and ZSM-22) is much higher than that of zeolites with three-dimensional structures [20-22]. In addition, compared with silicoaluminophosphate molecular sieves, one-dimensional zeolites demonstrate low preparation costs, which make them more appropriate for industrial applications [23,24]. Zschiesche *et al.* [25] compared the catalytic performance of C_{10}-C_{13} *n*-alkanes hydroisomerization over platinum-containing zeolite bifunctional catalysts with different one- and three-dimensional 10-（ZSM-5, ZSM-22, ZSM-23）and 12-membered-ring (Beta, HM and ZSM-12) pores. They found that among these acid supports, ZSM-12 zeolite with

MTW framework topology is considered as a very promising choice since its one-dimensional 12-membered rings pore system with a larger opening diameter of 0.56×0.62 nm is beneficial for improving diffusion properties of intermediate and products. The modified diffusion can result in suppression of the cracking of the isomer olefin intermediate and promotion of the formation of multi-branched isomer products. Pt/ZSM-12 exhibited the highest yields of total *iso*-alkanes (61.4 %) among all prepared bifunctional catalysts, in which maximum yields of mono- and multi-branched isomers achieved 35.3 % and 26.1 % at C_{10}-C_{13} *n*-alkane conversion of 78.0 %, respectively. Newalkar *et al.* [26] reported the effect of crystal morphology of ZSM-12 zeolite synthesized by using MTEABr, TEABr and BTMACl as templates respectively, on the catalytic performance for the hydroisomerization of *n*-hexadecane over the ZSM-12 loaded with 0.5 wt% Pt bifunctional catalysts. It is found that the catalyst based on TEABr-ZSM-12 with cuboidal (1–2 μm) presented higher isomer yield of 74.75 % at conversion of 86.06 %. However, for the practical applications of bifunctional catalysts, the yields of *iso*-alkanes was still unsatisfactory due to intensify cracking reaction of branched isomers in the hydroisomerization of longer carbon chain alkanes, and the properties of metal sites and the synergistic catalysis between metal and acid sites have not been investigated in these works.

The metal sites of bifunctional catalysts are generally provided by noble metals because of their excellent (de)hydrogenation functions and high selectivity for *iso*-alkanes [27]. The influences of metal sites have been investigated in detail by depositing various metal loadings or employing different calcination temperatures

[28,29]. It is worth noting that in many reported works, the content of supported noble metals is generally above 0.5 wt.%, which makes the cost of catalysts too expensive as a result. If the loadings of noble metal is not sufficient, the cracking of alkene intermediates will be intensified due to weak metal functions [30,31]. To date, there have been many attempts to decrease the noble metal loading (NML) of bifunctional catalysts, such as introducing transitional metals to form bimetallic sites [32,33]. However, high-temperature calcination and hydrogen reduction during the preparation process will lead to severe aggregation of metal particles, which results in a decrease of catalytic selectivity and stability. To effectively inhibit the aggregation of metal particles, the technology of "in-situ" encapsulation of noble metals in acid supports has been developed [34,35]. However, via this method, the metal precursor should be added into the initial gel for the synthesis of molecular sieves, which makes the synthesis process complicated and leads to a waste of noble metals.

Therefore, it is still very important to develop a novel and simple method to prepare bifunctional catalysts with low NML and excellent catalytic behaviours. In recent years, the in-situ plasma reduction at room temperature using argon glow discharge as a highly energetic electron source has captured wide attention due to its unique properties [36,37]. By employing this method, reduced metal nanoparticles show small size, high dispersion and excellent catalytic properties [38]. During the reduction process, no chemical reducing agents, protective chemicals or dispersing agents are needed [39]. Li *et al.* [40] prepared Pd/ZSM-22 catalysts via this method and found that the prepared catalysts demonstrate higher Pd dispersion, more

favourable metal-acid balance and improved catalytic performance for n-hexane hydroisomerization. However, there are still very few works about long-chain n-alkanes hydroisomerization over bifunctional catalysts prepared by the in-situ glow discharge plasma reduction method, especially for the purpose of improving the catalytic performance of bifunctional catalysts with a low NML, as well as increasing the selectivity of multi-branched isomers.

In this paper, we aim to establish a new method for the preparation of high-efficiency zeolite-based xPd/Z12-E bifunctional catalysts on the nanosized ZSM-12 zeolite with low noble metal loadings (0.1 wt.% and 0.3 wt.% Pd) for the hydroisomerization of n-hexadecane. The structure-performance relationships of prepared bifunctional catalysts are elucidated and the reasons for the highest iso-hexadecane yield of 80.2 % and selectivity for multi-branched isomers of 53.8 % over the 0.3Pd/Z12-E catalyst at n-hexadecane conversion of 93.6 % are also discussed. Different from the works reported by other scholars, we employ a novel in-situ room temperature electron reduction method to load Pd with higher dispersion and stronger ability to activate hydrogen than xPd/Z12-C catalysts prepared by the traditional hydrogen thermal reduction method. Moreover, the synthesized nano-ZSM-12 zeolite with larger openings size and abundant intergranular mesopores formed by the accumulation of small grains with an average size of approximately 40-50 nm is used as an acidic support, which can effectively improve the diffusion properties of iso-olefin intermediates and inhibit their cracking. With above modifications, more multi-branched iso-hexadecane in the n-hexadecane

hydroisomerization products at the maximum yield are obtained, which have excellent

low temperature flow properties as a second generation biodiesel component.

2. Experimental

2.1. Materials

The silica sol (32.3 wt.% SiO_2 in water, Qingdao Yumin, China), sodium

aluminate anhydrous ($NaAlO_2$, CP, Sinopharm, China), Sodium hydroxide (NaOH,

AR, Tianjin Guangfu, China) and Tetraethyl ammonium bromide (TEABr, AR,

Sinopharm, China) were used as silica, aluminium, alkaline source and template

respectively. The palladium nitrate solution (5 wt.% $Pd(NO_3)_2$, Shanxi Kaida, China)

was used as a noble metal precursor to prepare Pd/ZSM-12 bifunctional catalysts.

n-Hexadecane (AR, Tianjin Zhiyuan, China) was employed as the feed for the

catalytic test.

2.2. The preparation of ZSM-12 zeolite and Pd/ZSM-12 bifunctional catalysts

ZSM-12 zeolite was synthesized by the hydrothermal method and is described as

follows: TEABr, $NaAlO_2$ and silica sol were added into the NaOH solution under

stirring to form a mixture gel with the mole ratio of TEABr: Al_2O_3: SiO_2: Na_2O: H_2O

= 16.25: 1.0: 130: 4.225: 1690. The as-prepared mixture gel was then crystallized at

160 °C for 3 days. After crystallization, the obtained solids were filtered, washed,

dried overnight at 110 °C and then calcined in air at 650 °C. Then, the obtained

material was ion-exchanged in 0.5 M NH_4NO_3 aqueous solution at room temperature

for 3 h and calcined to obtain the HZSM-12 zeolite, which was denoted as the ZSM-12 sample.

To prepare the Pd/ZSM-12 catalysts, the ZSM-12 zeolite was first impregnated with an aqueous solution of $Pd(NO_3)_2$ and then dried for 12 h. Next, a part of the obtained sample was calcined at 600 °C for 4 h and then reduced with hydrogen at 400 °C for 1 h, which was named xPd/Z12-C, where x is the weight percentage of Pd loading (0.1 and 0.3 wt. %). The other part was treated by argon glow discharge plasma reduction for 1 h using a PB-1 plasma sputtering apparatus (Nanjing Suman Electronics Co., Ltd.). During the treatment, the sample was placed in a quartz discharge tube first and then treated at 70 Pa and room temperature. The prepared catalyst was denominated as xPd/Z12-E (x=0.1 wt. % and 0.3 wt. %).

2.3. Catalysts characterization

Powder X-ray diffraction (XRD) patterns were obtained using a Bruker D8 advance diffractometer over the 2θ range from 5 ° to 55 ° at a scanning speed of 2 °/min. The diffractometer used Cu Kα (λ=1.5406 Å) radiation (40 kV, 40 mA). The N_2 adsorption–desorptionan measurement was conducted using an Autosorb-iQ2 apparatus (Quantachrome Instruments) at -196 °C. Before adsorption, the sample was outgassed under a vacuum of 1.0×10^{-3} Pa for 12 h at 300 °C. The morphology of the ZSM-12 zeolite was determined by scanning electron microscopy (SEM) using a JSM-6480 A microscope operated at 20 kV. The TEM image and EDS mapping were characterized by a JEM-F200 microscope operating at 120 kV. The ^{27}Al and ^{29}Si MAS

NMR spectra were obtained using a Bruker Avance-400 spectrometer with a 4 mm

zirconia rotor operated at spinning rates of 10 kHz and 12 kHz, respectively. The

quantitative analysis of the Brønsted acid sites was accomplished by IR spectroscopy

of the adsorbed pyridine (Py-IR)(PE-100, PerkinElmer, USA) analysis. Prior to the

experiments, 20 mg of sample was dehydrated at 350 °C and 1.33×10^{-3} Pa for 2 h,

and pure pyridine gas was consequently adsorbed at 90 °C for 30 min. The total and

strong Brønsted acid sites density was investigated based on the area of the band at

approximately 1545 cm^{-1} in the IR spectra recorded during the desorption of pyridine

at 200 °C and 350 °C, respectively. The total Lewis acid sites density was determined

also by Py-IR method based on the area of the band at 1545 cm^{-1}. For quantification,

the corresponding extinction coefficient of 1.67 cm/µmol and 2.22 cm/µmol for

Brønsted and Lewis acid sites was employed, respectively [41,42]. The Pd dispersion

of all catalysts was measured by hydrogen chemisorption using a Micromeritics

AutoChem II 2920 Chemisorption Analyser instrument. The sample was reduced by

hydrogen at 400 °C for 1 h and then pretreated under argon flow at 450 °C for 2 h,

finally cooled to 35 °C and then exposed to pulses of a 10 % H_2-Ar mixture until

absorption saturation. The samples after adsorption saturation was further subjected to

H_2-TPD experiment in Ar flow with a heating rate of 10 °C/min.

2.4. Catalytic performance test

The hydroisomerization of *n*-hexadecane was conducted in a fixed-bed reactor

with a diameter of 10 mm. The reaction conditions were set as follows: the mass of

catalyst was 1 g (20~40 mesh), the reaction pressure was 2.0 MPa, the reaction temperature ranged between 240-320 °C, the flow of H_2 was 40 mL/min, and the weight hourly space velocity (WHSV) of n-hexadecane was 3.7 h^{-1}. Before the experiment, all catalysts were reduced by H_2 (40 ml/min) at 400 °C for 1 h. Product analysis was measured by using a gas chromatograph (Agilent 7820) with a flame ionization detector (FID) and an HP-1 capillary column (60 m × 250 μm × 1 μm). Conversion of n-C_{16}, selectivity of i-C_{16} (mono- or multi-branched), and yield of i-C_{16} were calculated using the following equations:

$$\text{Conversion of } n\text{-}C_{16} = \frac{n\text{-}C_{16} \text{ consumed}}{n\text{-}C_{16} \text{ in feedstock}} \tag{1}$$

$$\text{Selectivity of } i\text{-}C_{16} = \frac{i\text{-}C_{16} \text{ formed}}{n\text{-}C_{16} \text{ consumed}} \tag{2}$$

$$\text{Yield of } i\text{-}C_{16} = \frac{i\text{-}C_{16} \text{ formed}}{n\text{-}C_{16} \text{ in feedstock}} \tag{3}$$

3. Results and discussion

3.1. The physico-chemical properties of ZSM-12 zeolite and all Pd/Z12 bifunctional catalysts

The XRD pattern of the ZSM-12 zeolite is shown in Fig. 1a. The characteristic diffraction peaks observed at 2θ values of 7.6 °, 8.8 °, 20.9 °, 22.9 ° and 23.3 ° are assigned to the MTW topological structure (JCPDS No. 86-2364) [43]. Furthermore, no evidently additional peaks are observed, suggesting that the synthesized ZSM-12

zeolite is substantially free from impurities. In addition, diffraction peaks attached to

ZSM-12 zeolite were detected in all Pd/Z12 catalysts, and no Pd peaks were found

(shown in Fig. S1), suggesting a high dispersion of Pd nanoparticles. Tab. 1 lists the

relative crystallinity of all samples, which indicates that the loading of Pd will leads to

a decrease in relative crystallinity, especially for the 0.3Pd/Z12-C and 0.3Pd/Z12-E

catalysts prepared by loading 0.3 wt.% Pd. This phenomenon may originate from

defect formation in the ZSM-12 zeolite due to the etching effect of the acid $Pd(NO_3)_2$

solution during preparation process of the catalysts [44].
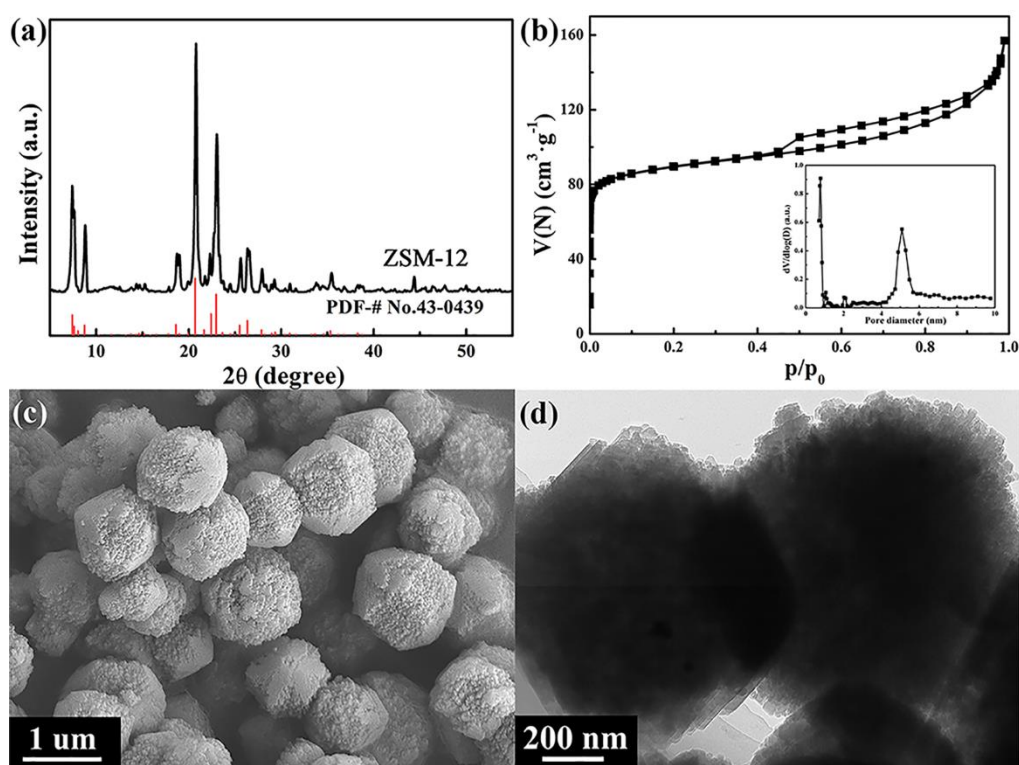
Figure 1. (a) The XRD pattern, (b) N_2 adsorption-desorption isotherm and pore

distribution (inset), (c) SEM image and (d) TEM image of the ZSM-12 zeolite.

Table 1. The textural properties of the ZSM-12 zeolite and all Pd/Z12 catalysts.

Sample	Relative crystallinity (%)	Surface area (m^2 g^{-1})			Pore volume (cm^3 g^{-1})		
		BET[a]	Micropore[b]	External	Total[c]	Micropore[b]	Mesopore
ZSM-12	100	345	285	60	0.243	0.113	0.130
0.1Pd/Z12-C	97	299	258	41	0.217	0.102	0.115
0.3Pd/Z12-C	82	261	221	40	0.217	0.088	0.129
0.1Pd/Z12-E	97	320	271	49	0.224	0.107	0.117
0.3Pd/Z12-E	82	294	245	49	0.221	0.097	0.124

Obtained by: [a] BET method, [b] t-plot method, [c] Volume adsorbed at $p/p_0 = 0.99$.

The N_2 adsorption-desorption isotherm, pore distribution and calculated textural properties of the ZSM-12 zeolite are shown in Fig. 1b and Tab. 1. The isotherm of ZSM-12 zeolite presents a combination of type-I and type-IV isotherms. The steep uptake at $p/p_0 = 0.01$ and the upswing at high relative pressure are attributed to the existence of micropores and multilayer adsorption, respectively. Simultaneously, the small hysteresis loop found in the isotherm is assigned to the intercrystal mesopores. The morphology of the synthesized ZSM-12 zeolite was observed by SEM and TEM measurements (Fig. 1c and 1d). The ZSM-12 zeolite exhibits a typical MTW morphology of irregular aggregate spheres approximately 1μm in diameter, which are composed of nanocrystals with an average size of approximately 40-50 nm. The N_2 adsorption-desorption isotherms and textural properties of all Pd/Z12 catalysts are demonstrated in Fig. S1 and Tab. 1. After the deposition of Pd nanoparticles, the relative crystallinity, micropore surface and volume of the xPd/Z12-C and xPd/Z12-E catalysts both decrease, and the mesopore volume increase accordingly as increasing Pd loading from 0.1 wt.% to 0.3 wt.%, which can be attributed to the blockage of partial pore mouths by the deposited Pd nanoparticles and formation of more

structural defects during preparation process of the catalysts by impregnation with higher concentration of $Pd(NO_3)_2$ solution and its calcination. This is consistent with the results of decreasing relative crystallinity and increasing framework Si/Al ratio obtained by ^{29}Si MAS NMR characterization (Fig. S3). Moreover, the micropore surface area and volume of xPd/Z12-E catalysts are both larger than that of the xPd/Z12-C catalysts with the same Pd loading, suggesting that the employment of the plasma reduction method can reduce the damaged degree of the micropore channel under the room temperature electron reduction conditions.

Beyond the textural property, the Brønsted acidity is another significant impact factor of the catalytic performance. The Brønsted acid density of the ZSM-12 zeolite and Pd/Z12 catalyst was measured by Py-IR measurement. The spectra and the calculated results are presented in Fig. S4 and Tab. 2, respectively. As presented in Tab. 2, the total Brønsted acid density of all catalysts loaded Pd is lower than the ZSM-12 zeolite, and decreases in Brønsted acid sites and distribution of Brønsted acid sites in the total acid sites (Table S1) as the increasing Pd loading due to the blockage of more micropores or coverage of more Brønsted acid sites. The 0.3Pd/Z12-E catalyst demonstrates the lowest Brønsted acid density among the four catalysts, which may be related to the highest Pd dispersion and more Brønsted acid sites covered.

Table 2. The Brønsted acid density and metal characteristics of ZSM-12 zeolite and all Pd/Z12 catalysts.

Sample	Brønsted acid sites (μmol g^{-1})		D_{Pd} (%)[a]	C_{Pd} (μmol g^{-1})[b]	C_{Pd}/C_{H+}[c]	Pd size (nm)[d]
	Strong	Total				
ZSM-12	23.5	27.3	-	-	-	-
0.1Pd/Z12-C	22.0	26.2	8.9	0.84	0.032	12.5
0.3Pd/Z12-C	20.5	25.1	14.3	4.03	0.161	7.8
0.1Pd/Z12-E	21.1	25.4	14.4	1.35	0.053	7.8
0.3Pd/Z12-E	18.1	23.3	28.5	8.03	0.345	3.9

[a] Determined by H_2 chemisorption, [b] Calculated by Pd dispersion, [c] Calculated by total Brønsted acid sites, [d] Determined by the chemisorption method.

To compare the dispersion of the Pd nanoparticles on the catalysts prepared with different Pd loadings by glow discharge plasma reduction and conventional hydrogenation reduction method, the H_2 chemisorption were measured, and the results are also shown in Tab. 2. It is found that the Pd dispersion of two series of bifunctional catalysts improves with the increase of Pd loadings. The Pd dispersion of the *x*Pd/Z12-E catalysts is significantly larger than that of the corresponding *x*Pd/Z12-C catalysts with same Pd loadings. In particular, the 0.3Pd/Z12-E catalyst shows an almost 2 times larger Pd dispersion compared to the 0.3Pd/Z12-C catalyst. This result demonstrates that the glow discharge plasma reduction method can markedly improve the Pd dispersion, and the Pd nanoparticles size is accordingly smaller. There are two reasons for this result: a) the interaction between the ZSM-12 zeolite and Pd nanoparticles is strongly enhanced by highly energetic electrons generated during the reduction process; b) in-situ the glow discharge plasma reduction at room temperature to prepare the *x*Pd/Z12-E catalysts can significantly inhibit the aggregation of Pd nanoparticles, that occurs during the calcination process of *x*Pd/Z12-C catalysts at higher temperature [45]. Moreover, the ratio of exposed Pd

active sites to total Brønsted acid density (C_{Pd}/C_{H+}) is also calculated, which generally represents the balance degree between metal function and acid function. Notably, the C_{Pd}/C_{H+} ratio of the 0.3Pd/Z12-E catalyst (0.345) is approximately 2.2 times higher than that of the 0.3Pd/Z12-C catalyst (0.161).

Since the Pd nanoparticles on the *x*Pd/Z12-E catalysts are directly reduced from Pd(NO$_3$)$_2$ impregnated on the ZSM-12 zeolite by glow discharge plasma in the preparation process, only unreduced *x*Pd/Z12-C catalysts after calcination are characterized by H$_2$-TPR to to explain the effect of Pd loadings on the dispersion, and the results are shown in Fig. 2. The two peaks below 50 °C for the two catalysts are ascribed to the reduction of small PdO nanoparticles on the surface, which are easier to be reduced due to the weak interaction with the support [46]. The negative peak observed at 68 °C for the 0.3Pd/Z12-C catalyst is assigned to the decomposition of β-PdH formed on metallic Pd particles reduced from large PdO particles [47]. While for the 0.1Pd/Z12-C catalyst, the disappearance of the corresponding negative peak may be due to overlap of this peak with the reduction peak at 48 °C [48]. In addition, the reduction peaks at 340 °C and above 400 °C for the two catalysts are attributed to the reduction of PdO particles in the main micropores and the Pd^{2+} locateded on the ion-exchanged position, respectively [47]. For the 0.3Pd/Z12-C catalyst, the peak occurs at a higher reduction temperature (at 554 °C) than that of 0.1Pd/Z12-C, indicating there is a stronger interaction between Pd^{2+} ions in the unreduced 0.3Pd/Z12-C catalyst and the negatively charged skeleton of the ZSM-12 zeolite with more framework defect sites, so that the 0.3Pd/Z12-C catalyst demonstrates a much

higher Pd dispersion [49].
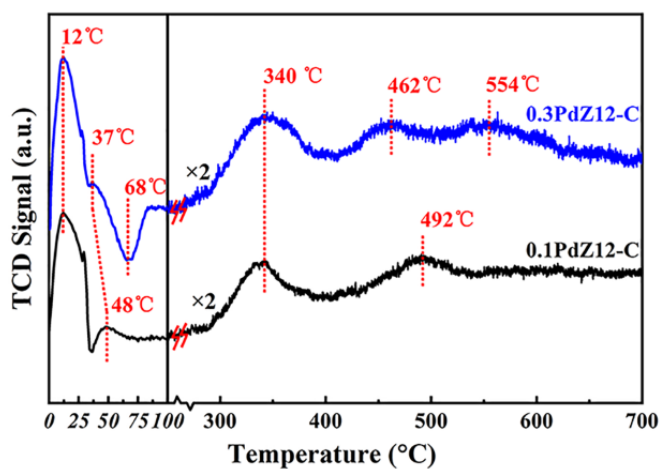
Figure 2. H_2-TPR profiles of 0.1Pd/Z12-C and 0.3Pd/Z12-C catalysts

To further investigate the Pd dispersion on the catalysts prepared by the two methods, two catalysts with the Pd loading of 0.3 wt.% were characterized by TEM measurement due to Pd nanoparticles were difficult to observe on the catalysts loaded with 0.1 wt.% Pd. According to the TEM image and EDS mapping (Fig. 3), the Pd nanoparticles are dispersed well on the ZSM-12 zeolite for the two catalysts, and the average size of the Pd nanoparticles on the 0.3Pd/Z12-E catalyst is approximately 3.1 nm, which is visibly smaller than that of the 0.3Pd/Z12-C (7.2 nm). Aiken and Wang reported that the corners and defects of metal nanoparticles increase as their size decreases, which effectively promotes metal function [50,51]. Furthermore, the high-resolution TEM images shown in Fig. S5 demonstrate that Pd (111) and Pd (100) facets with lattice fringes of 0.23 nm and 0.20 nm can be observed, respectively, in the 0.3Pd/Z12-C catalyst. While for the 0.3Pd/Z12-E catalyst, more lattice fringes ascribed to the Pd (111) facet are found. This phenomenon suggests that the glow

discharge plasma reduction method can increase the proportion of Pd (111) facets, which is consistent with reported results about Pd/ZSM-22 and Pt/C catalysts [40,52].
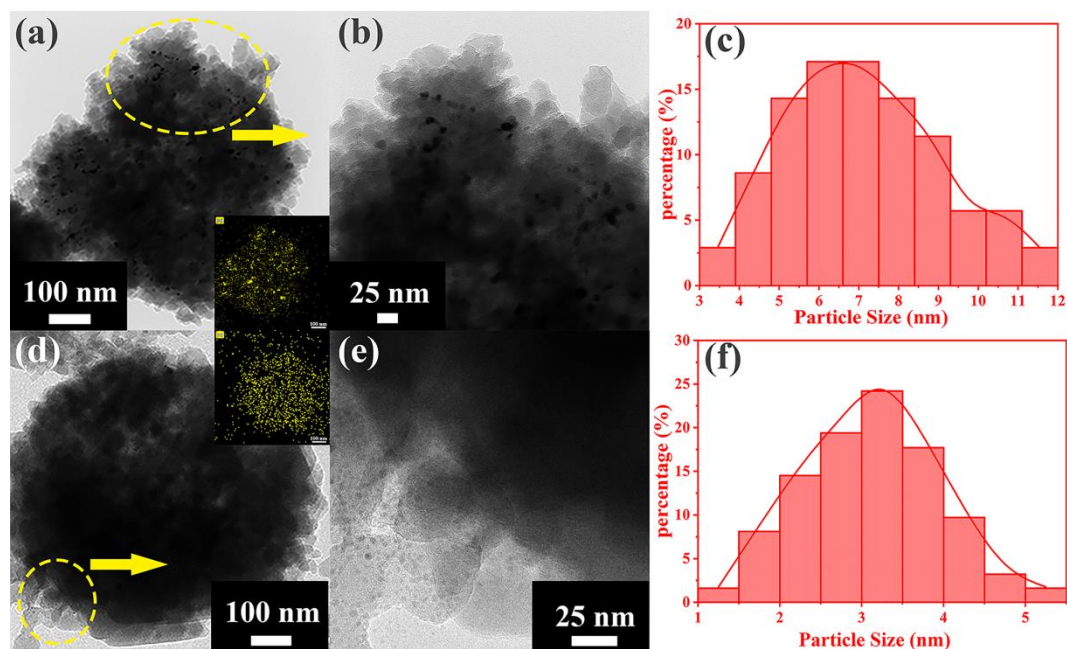
Figure 3. TEM images, EDS mapping and Pd size distribution of (a-c) 0.3Pd/Z12-C and (d-f) 0.3Pd/Z12-E catalysts.

Beyond the TEM images, the influence of the reduction method on the Pd different facet distribution was further investigated by CO adsorbed FT-IR. Since the band is too weak to be observed for the 0.1Pd/Z12-C and 0.1Pd/Z12-E catalysts due to the very low Pd loading, Fig. 4a only shows the CO adsorbed FT-IR spectra of the 0.3Pd/Z12-C and 0.3Pd/Z12-E catalysts. CO gas bands at 2143 cm^{-1} and 2134 cm^{-1}, the top CO-Pd (111) bands at 2082 cm^{-1} and 2063 cm^{-1}, the bridge CO-Pd (100) band at 2025 cm^{-1} and the bridge CO-Pd (111) band at 2004 cm^{-1} are all observed for the two catalysts [53]. Notably, the area ratio of the bridge CO-Pd (111) band and the bridge CO-Pd (100) band for the 0.3Pd/Z12-E catalyst (1.6) is higher than that of the 0.3Pd/Z12-C catalyst (1.3). This phenomenon demonstrates that the proportion of the

Pd (111) facet of the catalyst prepared by in-situ glow discharge plasma reduction is evidently enhanced compared with that of the catalyst prepared by hydrogen reduction with the same Pd loading, which is consistent with the TEM results. The difference in crystal facet distribution can be attributed to the different mechanisms of crystal growth during the Pd reduction processes. For the xPd/Z12-E catalysts, the excitation of high energetic electrons of glow discharge leads to more nucleation of Pd seeds [54]. Simultaneously, the room temperature condition makes it hard for the migration of Pd atoms. Therefore, the Pd seeds will grow slowly to the octahedral or tetrahedral shape and expose more Pd (111) facet, which is the kinetic controlled mechanism. While the xPd/Z12-C catalysts forms fewer Pd seed crystals during the reduction process, and the migration of Pd atoms becomes much easier at high reduction temperatures. Therefore, the crystal growth of Pd seeds is much faster, and the growth mechanism is controlled by thermodynamics. Then, the Pd nanoparticles grow into a truncated octahedron shape with more Pd (100) facets [55,56]. In order to further investigate the ability of the catalysts to adsorb and activate hydrogen, the H_2-TPD of all catalysts was measured, and the results are shown in Fig. 4b and S6. The H_2 desorption temperature for the xPd/Z12-E catalysts is higher than that of the corresponding xPd/Z12-C catalysts. According to Kyriakou's work, if the H_2 dissociation barrier is lower on the metal sites, the binding energy of dissociated H atoms will be higher, which will lead to hard desorption of H_2 [57]. Therefore, the higher H_2 desorption temperature of xPd/Z12-E catalysts suggests that the activation and dissociation of H_2 on their Pd sites are easier, which means a stronger

hydrogenation function than that of xPd/Z12-C catalysts. Therefore, xPd/Z12-E catalysts prepared by in-situ glow discharge plasma reduction not only has a higher Pd dispersion, larger C_{Pd}/C_{H+} ratio, but also has stronger function of hydrogen activation originated from exposure of more (111) facets, which may be enhance the catalytic performance.
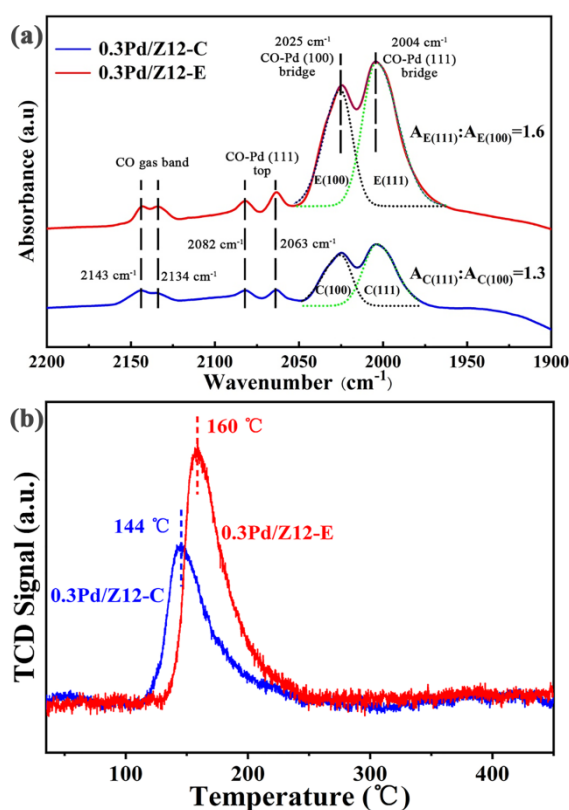

Figure 4. (a) The CO adsorbed FITR spectra and (b) H$_2$-TPD curve of 0.3Pd/Z12-C and 0.3PdZ12-E catalysts.

3.2. The catalytic performance for the hydroisomerization of n-hexadecane

For bifunctional catalysts, it is well known that the metal-acid balance has significant effects on the catalytic performance. Therefore, to further discuss the effects of reduction methods on metal function as well as catalytic performance, the

n-hexadecane hydroisomerization was tested over two series of bifunctional catalysts loaded Pd on the ZSM-12 zeolite. Fig. 5a presents the conversion of *n*-hexadecane versus the reaction temperature, and well-matched S-shaped curves are observed for all catalysts. The conversion of *n*-hexadecane over all catalysts increases gradually with the rise of the reaction temperature.

In addition, the relationships between *n*-hexadecane conversion and Brønsted acid density (C_{H+}), exposed Pd active sites density (C_{Pd}) and C_{Pd}/C_{H+} ratio are correlated to further investigate the influence factors of the catalytic activity. Fig. 5b show the relationships at 260 °C (in the dynamic controlled range) and 300 °C (in the thermodynamically controlled range), respectively. It can be found that the *n*-hexadecane conversion is enhanced with the increase of Brønsted acid density of the catalysts at reaction temperature of 260 °C. However, when the C_{Pd} and C_{Pd}/C_{H+} ratio increase, the *n*-hexadecane conversion reduces (Fig. 5c-d) due to a corresponding decrease of Brønsted acid density with increase of exposed Pd active sites. Therefore, in the dynamic controlled range, skeletal isomerization and cracking reactions on the acid sites of the bifunctional catalyst are the rate-controlling steps of the reaction, and the Brønsted acid density is the main influence factor of the activity of the bifunctional catalysts.
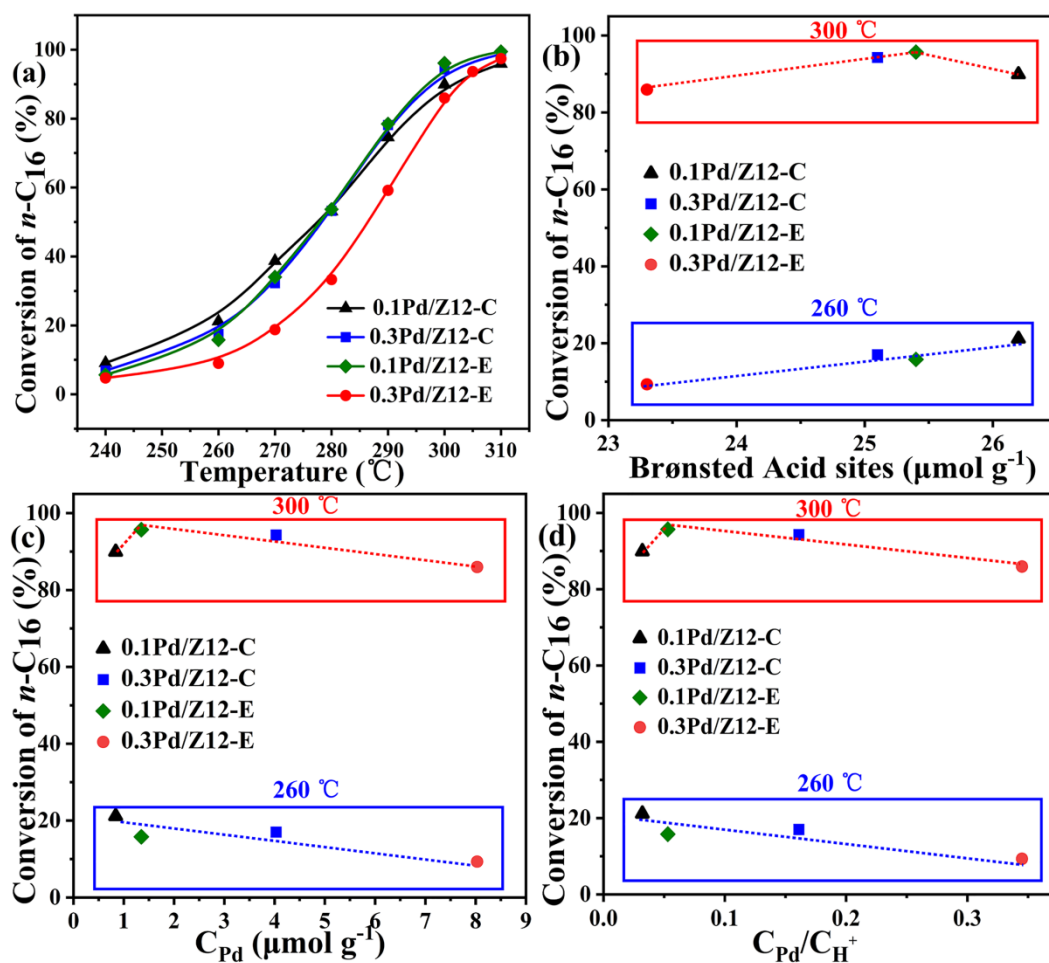
Figure 5. The relationships between *n*-hexadecane conversion and reaction temperature (a), C_{H+} (b), C_{Pd} (c) and C_{Pd}/C_{H+} ratio (d)

However, while the temperature becomes 300 °C, the *n*-hexadecane conversion over the 0.1Pd/Z12-C catalyst does not follow the rules obtained at 260 °C. Although the 0.1Pd/Z12-C catalyst has the largest acid density, the amount of exposed Pd sites of the 0.1Pd/Z12-C catalyst is too low to adsorb and activate hydrogen since the chemical adsorption of hydrogen on Pd sites at higher temperature will be weakened for all catalysts. Accordingly, the 0.1Pd/Z12-C catalyst shows the lower activity than that of the 0.1Pd/Z12-E catalyst with lower Brønsted acid density. Therefore, in the thermodynamic controlled range, when the metal site density of the catalyst is insufficient, the catalytic dehydrogenation of *n*-alkanes and the hydrogenation of

iso-alkenes intermediates on the metal sites are the rate-controlling steps for the hydroisomerization of *n*-alkanes, and the density of exposed Pd active sites has more important influence to the activity of the bifunctional catalysts. The 0.1Pd/Z12-E catalyst shows the highest *n*-hexadecane conversion in thermodynamically controlled range due to synergistic catalysis of metal and acid sites, which is originated from higher Brønsted acid density, sufficient Pd active sites as well as enhanced hydrogen activation ability.

In addition to the catalytic activity, the selectivity for branched isomers, and products distribution are more important evaluation parameters of the bifunctional catalysts for the hydroisomerization of long-chain *n*-alkanes, especially for multi-branched isomers, which are expected to be used as green biodiesel component with excellent low temperature fluidity. Therfore, the relationships between *iso*-hexadecane yield and conversion, C_{H+} and C_{Pd}/C_{H+} ratio are investigated to further discuss the impact factors of *iso*-hexadecane yield over two series of catalysts at *n*-hexadecane conversion ~ 95 % (in the thermodynamically controlled range, in which more multi-branched isomers will be generated). Simultaneously, the products distribution at representative conversions (~ 20 %, ~ 50% and ~ 95 %) are also compared and the results were shown in Figure 6.

Figure 6. The relationships between *iso*-hexadecane yield and *n*-hexadecane conversion (a); *iso*-hexadecane yield *vs* C_{H+} (b) and C_{Pd}/C_{H+} ratio (c) at *n*-hexadecane conversion of ~ 95 % ; the distribution of *iso*-hexadecane over different catalysts at *n*-hexadecane conversion of ~ 20 % (d), ~ 50 % (e) and ~ 95 % (f).

From Figure 6a, although the 0.3Pd/Z12-E catalyst has the lowest activity among all catalysts at the same tempereture, there is no significant difference in *iso*-hexadecane yield when the *n*-hexadecane conversion is lower than ~20 % (in dynamic controlled range), except for the 0.1Pd/Z12-C catalyst with minimum matal sites density. The low *iso*-hexadecane yield over the 0.1Pd/Z12-C catalyst can be explained by its maximum n_{as} value of 2.28, which represents the average number of acid sites of one *n*-hexadecane molecule contacted during the hydroisomerization reaction between two adjacent metal sites, calculated based on the reaction results at *n*-hexadecane conversion of ~20 % (Table S2). It is found that the n_{as} value of the 0.1Pd/Z12-C catalyst is greater than that of 0.3Pd/Z12-C (1.87), 0.1Pd/Z12-E (1.66)

and 0.3Pd/Z12-E (1.48), indicating that stronger cracking reactions even appeared at lower temperatures (corresponding conversion is less than ~20 %) when the metal sites are severely deficient. It is worth noting that, there is a greater difference in the *iso*-hexadecane yield over two series of catalysts in thermodynamic controlled range (at *n*-hexadecane conversion of 80~95 %). Figure 6b, 6c present that the reduced C_{H+} and increased C_{Pd}/C_{H+} ratio are both beneficial for improving the *iso*-hexadecane yield. For the 0.1Pd/Z12-C catalyst with highest Brønsted acid density and lowest C_{Pd}/C_{H+} ratio, the maximum *iso*-hexadecane yield is only 65.8 % at *n*-hexadecane conversion of 89.9 % due to the lack of metal sites and weak hydrogenation function, resulting in strong cracking of isomeric alkene intermediates on the Brønsted acid sites. While for the 0.3Pd/Z12-C catalyst, the metal function is effectively improved because of the increase of Pd loading from 0.1 wt.% to 0.3 wt.%, as well as the Pd dispersion (from 8.9 % to 14.3 %) and the C_{Pd}/C_{H+} ratio (from 0.027 to 0.161). Accordingly, an increased *iso*-hexadecane yield of 72.8 % is achieved over the 0.3Pd/Z12-C catalyst at *n*-hexadecane conversion of 94.3 %. For the *x*Pd/Z12-E series of catalysts, the *iso*-hexadecane yield is also significantly improved when Pd loading increases from 0.1 wt.% to 0.3 wt.%, as well as the C_{Pd}/C_{H+} ratio correspondingly increases from 0.053 to 0.345. The *x*Pd/Z12-E series of catalysts present obviously higher maximum *iso*-hexadecane yield than that of *x*Pd/Z12-C catalysts with same Pd loading at conversion of ~95%, which can be explained by the following reasons. First, *x*Pd/Z12-E catalysts have larger Pd sites density and C_{Pd}/C_{H+} ratio, which is 1.7~2.1 times more than that of *x*Pd/Z12-C series of catalysts with the same Pd

loading, which will facilitate hydrogenation of *iso*-alkene intermediates to *iso*-hexadecane rather than further cracking into light hydrocarbons. Furthermore, *x*Pd/Z12-E catalysts expose more Pd (111) facets because of the kinetically controlled growth mechanism for the Pd nanoparticles, which leads to a much stronger H_2 chemical adsorption and dissociation capacity compared with *x*Pd/Z12-C series catalysts with exposure of more Pd (100) facets [58]. It is noteworthy that the maximum yield of *iso*-hexadecane achieved over the 0.1Pd/Z12-E catalyst with 0.1 wt.% Pd loading (C_{Pd}/C_{H+} = 0.053) is close to that obtained on a 0.3Pd/Z12-C catalyst with three times the Pd loading (C_{Pd}/C_{H+} = 0.161), which demonstrates that, compared with the C_{Pd}/C_{H+} ratio, the stronger hydrogen activation capacity of the 0.1Pd/Z12-E catalyst is a more important factor for improving the yield of *iso*-hexadecane. While the highest *iso*-hexadecane yield of 80.2 % at at *n*-hexadecane conversion of 93.6 % is obtained over the 0.3Pd/Z12-E catalyst with 0.3 wt.% Pd loading, which can be attributed to synergistic effect of the largest C_{Pd}/C_{H+} ratio and the stronger hydrogenation capability provided by the more Pd (111) facets. This highest yield is a relatively high level among some reported zeolite-based bifunctional catalysts prepared with larger metal loading (listed in Tab. S3). Therefore, the glow discharge plasma reduction method can significantly improve the catalytic behaviours of prepared catalysts for *n*-hexadecane hydroisomerization.

In order to clarify the change of catalytic performance at different *n*-hexadecane conversion, the distribution of mono-branched, multi-branched *iso*-hexadecanes and cracked products over all catalysts are compared at conversion of ~20 %, ~50 % and

~95 %, respectively, and the results are shown in Figure 6 and Figure S7, S8. It is found that, for each series of catalysts, the higher selectivity of mono-branched isomers and less cracked products are achieved over the catalysts with more Pd loading due to the greater metal active sites density and C_{Pd}/C_{H+} ratio. The mono-branched iso-hexadecanes are mainly products over all catalysts at ~20 % and ~50 % conversion. However, the selectivity of mono-branched isomers tends to decrease with increase of conversion, and multi-branched isomers enhanced accordingly. When the n-hexadecane conversion reach to about 95 %, the selectivity for multi-branched iso-hexadecane over all catalysts are maximum, which is about 2 times higher than that of mono-branched isomers. This result can be attributed to the improvement of diffusion properties of multi-branched iso-alkene intermediates because of abundant intergranular mesopores formed by the accumulation of ZSM-12 zeolite nanoparticle and the hence inhibition of its further cracking. In addition, the selectivity for cracked products at conversion of ~95 % is highest for each catalysts due to the intensify cracking of iso-olefin intermediate at corresponding higher temperatures. The xPd/Z12-E catalysts demonstrate higher selectivity for both mono-branched and multi-branched iso-hexadecane, and lower selectivity for craking products than those of the xPd/Z12-C catalysts with the same Pd loading at a similar conversion, which can be originated from the promoted hydrogenation of branched iso-alkene intermediates to form iso-hexadecane on Pd active sites caused by the enhanced metal function and synergistic catalysis of metal-acid sites [44]. The law of cracked products distribution is the same at different conversion over all catalysts, and

the distribution of the C_3-C_6 light hydrocarbon as well as the C_4/C_{12} and C_5/C_{11} values obtained at *n*-hexadecane conversion ~95% over the four catalysts decreases in the order of 0.1Pd/Z12-C > 0.3Pd/Z12-C > 0.1Pd/Z12-E > 0.3Pd/Z12-E (shown in Fig. S8 and Tab. S4), suggesting that the secondary cracking is reduced over the *x*Pd/Z12-E catalysts due to the enhanced metal function and synergistic catalysis between the metal sites and acid sites.

From the product distribution of mono-branched *iso*-hexadecane over two series of catalysts (Fig. S9), it can be seen that the distribution law for all catalysts is similar, and the proportion of 2-methylpentadecane is much less than that of mono-branched *iso*-hexadecanes with a centrally located branch. This result is attributed to the fact that the reaction mechanism of *n*-alkanes hydroisomerization is mainly determined by the textural properties of the molecular sieves that provide the acid sites of the bifunctional catalysts. All catalysts are prepared by using nano-ZSM-12 zeolite as the acidic support. The larger pore size of nano-ZSM-12 zeolite (opening diameter of 0.56×0.62 nm) is slightly larger than the dynamic diameter of the mono-branched isomers, which allows the *n*-hexadecane molecules to diffuse deep into the micropore channels to be isomerized and diffuse out of the pore channels fast to generate more 3-methyl- ~ 8-methylpentadecane products with a centrally located branch. Therefore, the hydroisomerization of *n*-hexadecane over all catalysts based on nano-ZSM-12 zeolite follows the "key-lock" mechanism.

For industrial applications of bifunctional catalysts, their catalytic stability is

very significant evaluation index. To investigate the effects of the metal function of

the catalysts prepared by different reduction methods on the catalytic stability, the

0.1Pd/Z12-C and 0.1Pd/Z12-E catalysts with only 0.1 wt.% Pd loading, which may be

more sensitive for the long-term tests, were used for stability investigation. As shown

in Fig. 7, the *n*-hexadecane conversion and selectivity for *iso*-hexadecane over the two

catalysts can be retained after 100 h of durability test. In addition, for the spent

0.1Pd/Z12-E catalyst, the dispersion decreased slightly, and the micropore volume

decreased much less than that of 0.1Pd/Z12-C catalyst (Table S5), indicating that the

pore blockage caused by carbon deposition was effectively inhibited, which can be

proved by TG curves of two spent catalysts (Fig. 8).
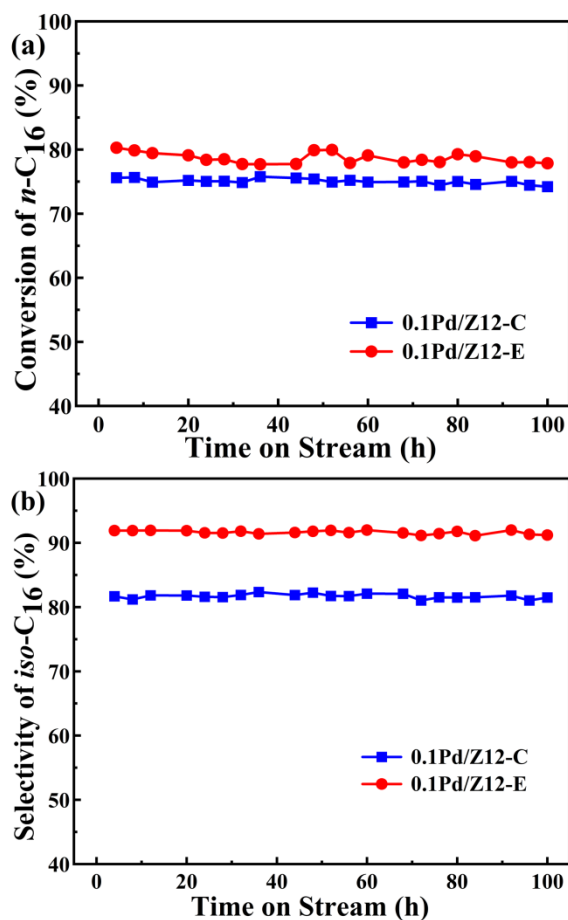
Figure 7. *n*-hexadecane conversion (a) and selectivity of *iso*-hexadecane (b) over the 0.1Pd/Z12-C and 0.1Pd/Z12-E catalysts as a function of the stream time.

From Fig. 8 can be seen, for the spent 0.1Pd/Z12-E catalyst, only a weight loss peak attributed to desorption of adsorbed water is observed between 100 ^{o}C and 150 ^{o}C, and there is no apparent weight loss of deposited carbon at higher temperature. However, for the used 0.1Pd/Z12-C catalyst, a weight loss (0.9 %) of deposited carbon is also appeared between 600 °C and 750 °C besides the weight loss of adsorbed water. Therefore, the employment of glow discharge plasma reduction is beneficial for the inhibition of carbon deposition and Pd aggregation on the bifunctional catalysts to maintain outstanding catalytic stability.
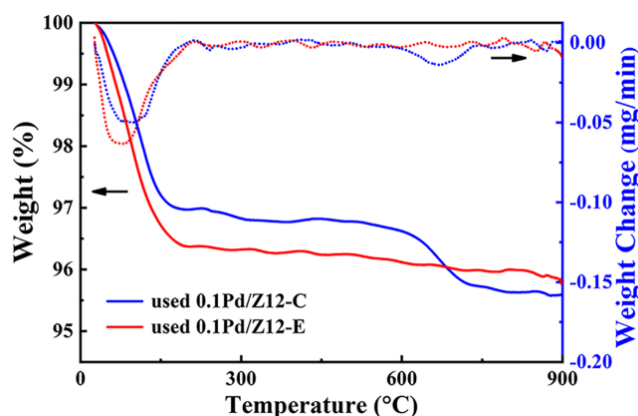
Figure 8. The TG and DSC curves of used 0.1Pd/Z12-C and used 0.1Pd/Z12-E catalysts

4. Conclusions

*x*Pd/Z12-E Bifunctional catalysts with 0.1 wt.% and 0.3 wt.% Pd loaded on nanosized ZSM-12 zeolite are prepared by novel in-situ glow discharge plasma reduction method at room temperature. Compared with *x*Pd/Z12-C catalysts with the

same Pd loadings prepared by the conventional hydrogenation reduction method, xPd/Z12-E catalysts present higher Pd dispersion and more exposed Pd (111) facets.

Based on the research results of catalytic performance for the n-hexadecane hydroisomerization obtained at different temperature ranges, we find that the density of Pd active sites and hydrogen activation ability have more significant influences to the catalystic activity than that of the acidity at higher reaction temperature (in the thermodynamically controlled range). Moreover, the stronger hydrogen activation ability caused by more exposed Pd (111) facets is more important compared with the larger ratio of metal to acid sites (C_{Pd}/C_{H+}) for the improvement of the catalytic performance. Accordingly, the maximum yield of iso-hexadecane achieved over the 0.1Pd/Z12-E catalyst with 0.1 wt.% Pd loading ($C_{Pd}/C_{H+} = 0.053$) is close to that obtained over the 0.3Pd/Z12-C catalyst with three times the Pd loading ($C_{Pd}/C_{H+} = 0.161$). Furthermore, xPd/Z12-E series of catalysts show higher yield of iso-hexadecane and selectivity for multi-branched isomers, as well as excellent catalytic stability, due to the stronger hydrogen activation ability and favourable metal-acid balance. The maximum iso-hexadecane yield of 80.2 % and selectivity for multi-branched iso-hexadecane of 53.8 % at n-hexadecane conversion of 93.6 % was obtained over the 0.3Pd/Z12-E catalyst.

Therefore, the in-situ glow discharge plasma reduction is an effective method to prepare highly effective bifunctional catalysts with a low noble metal loading and excellent catalytic performance for the hydroisomerization of long-chain n-alkanes,

which show a further industrial application potential for production of second generation biodiesel with outstanding low-temperature fluidity.

Acknowledgement

Reference

1. Cheng K, van der Wal LI, Yoshida H, Oenema J, Harmel J, Zhang Z, et al. Impact of the spatial organization of bifunctional metal-zeolite catalysts for hydroisomerization of light alkanes. Angew Chem Int Ed 2020;59:3592–3600.

2. Zecevic J, Vanbutsele G, de Jong KP, Martens JA. Nanoscale intimacy in bifunctional catalysts for selective conversion of hydrocarbons. Nature 2015;528:245–254.

3. Satar I, Isahak WNRW, Salimon J. Characterization of biodiesel from second generation gamma-irradiated Jatropha curcas. J Taiwan Inst Chem E 2015;49: 85–89.

4. Singh D, Sharma D, Soni S L, Sharma S, Sharma P K, Jhalani A. A review on feedstocks, production processes, and yield for different generations of biodiesel. Fuel 2020;262:116553.

5. Perez W, Marin J, del Rio J, Pena J, Rios L. Upgrading of palm oil renewable diesel through hydroisomerization and formulation of an optimal blend. Fuel 2017;209:442–448.

6. Singh D, Sharma D, Soni S L, Inda C S, Sharma S, Sharma P K, et al. A comprehensive review of physicochemical properties, production process,

performance and emissions characteristics of 2nd generation biodiesel feedstock: Jatropha curcas. Fuel 2021;285:119110.
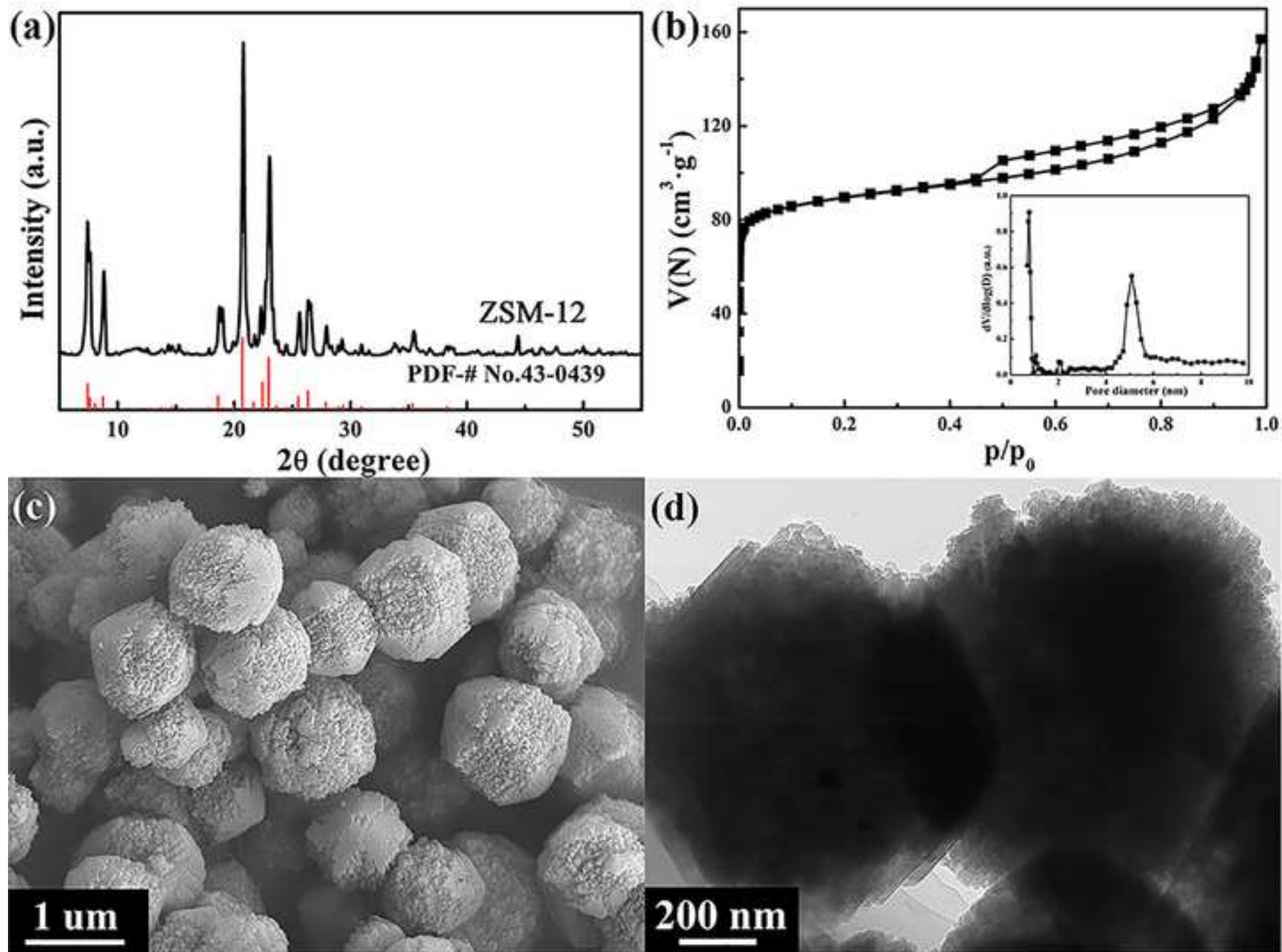
7. Singh D, Sharma D, Soni SL, Sharma S, Kumari D. Chemical compositions, properties, and standards for different generation biodiesels: a review. Fuel 2019;253:60–71.

8. Shumeiko B, Auersvald M, Straka P, Simacek P, Vrtiska D, Kubicka D. Efficient one-stage bio-oil upgrading over sulfided catalysts. ACS Sustainable Chem Eng 2020;8:15149–15167.

9. Chen LY, Chen YH, Hung YS, Chiang TH, Tsai CH. Fuel properties and combustion characteristics of jatropha oil biodiesel–diesel blends. J Taiwan Inst Chem E 2013;44:214–220.

10. Zhang M, Li C, Chen X, Chen Y, Liang C. Hierarchical ZSM-48-supported nickel catalysts with enhanced hydroisomerization performance of hexadecane. Ind Eng Chem Res 2019;58:19855–19861.

11. Zhang M, Chen Y, Wang L, Zhang Q, Tsang C W, Liang C. Shape selectivity in hydroisomerization of hexadecane over Pt supported on 10-ring zeolites: ZSM-22, ZSM-23, ZSM-35, and ZSM-48. Ind Eng Chem Res 2016;55:6069–6078.

12. Tao S, Li X, Wang X, Wei Y, Jia Y, Ju J, et al. Facile synthesis of hierarchical nanosized single-crystal aluminophosphate molecular sieves from highly homogeneous and concentrated precursors. Angew Chem Int Ed 2020;59:3455–3459.

13. Zanatta ER, Reinehr TO, Barros JLM, da Silva EA, Arroyo PA. Hydroisomerization of n-hexadecane under mesoporous molecular sieve Pt/Al-SBA-15. Mol Catal 2021;512:111737.

14. Yang L, Wang W, Song X, Bai X, Feng Z, Liu T, et al. The hydroisomerization of n-decane over Pd/SAPO-11 bifunctional catalysts: The effects of templates on characteristics and catalytic performances. Fuel Process Technol 2019;190:13–20.

15. Harmel J, Roberts T, Zhang Z, Sunley G, de Jongh P, de Jong KP. Bifunctional molybdenum oxide/acid catalysts for hydroisomerization of n-heptane. J Catal 2020;390:161–169.

16. Jin D, Ye G, Zheng J, Yang W, Zhu KK, Coppens MO, et al. Hierarchical silicoaluminophosphate catalysts with enhanced hydroisomerization selectivity by directing the orientated assembly of premanufactured building blocks. ACS Catal 2017;7:5887–5902.

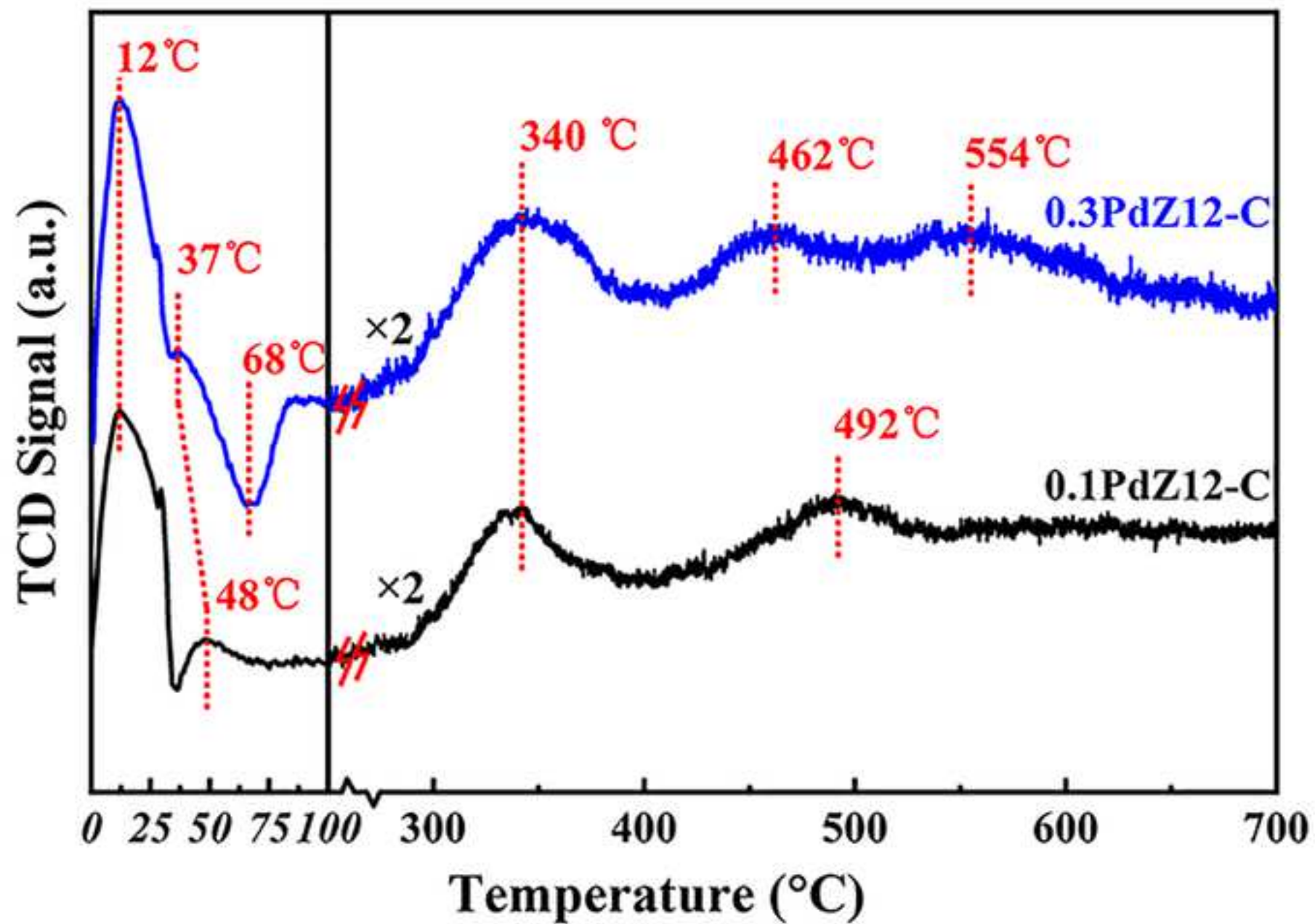17. Lyu Y, Yu Z, Yang Y, Liu Y, Zhao X, Liu X, et al. Metal and Acid Sites Instantaneously Prepared over Ni/SAPO-11 Bifunctional Catalyst. J Catal 2019;374:208–216.

18. Kim J, Han SW, Kim J–C, Ryoo R. Supporting nickel to replace platinum on zeolite nanosponges for catalytic hydroisomerization of *n*-dodecane. ACS Catal 2018;8:10545–10554.

19. Kumar SK, John M, Pai SM, Ghosh S, Newalkar BL, Pant KK. Selective hydroalkylation of benzene over palladium supported Y-Zeolite: Effect of metal acid balance. Mol Catal 2017;442:27–38.

20. Pastvova J, Kaucky D, Moravkova J, Rathousky J, Sklenak S, Vorokhta M, et al. Effect of enhanced accessibility of acid sites in micromesoporous mordenite zeolites on hydroisomerization of *n*-hexane. ACS Catal 2017;7:5781–5795.

21. Gopal S, Zhang W, Smirniotis PG. Comparison of hydroisomerization and hydrocracking reactions of normal and branched octanes over USY and ZSM-12 catalysts. Ind Eng Chem Res 2004;43:2950–2956.

22. Zhang L, Fu W, He L, Cai G, Chen Q, Tang T. Design and synthesis of Pt catalyst supported on ZSM-22 nanocrystals with increased accessible 10-MR pore mouths and acidic sites for long-chain *n*-alkane hydroisomerization. Micropor Mesopor Mater 2021;313:110834.

23. Nghiem VT, Sapaly G, Meriaudeau P, Naccache C. Monodimensional tubular medium pore molecular sieves for selective hydroisomerisation of long chain alkanes: *n*-octane reaction on ZSM and SAPO type catalysts. Top Catal 2000;14:131–138.

24. Feng Z, Wang W, Wang Y, Bai X, Su X, Yang L, et al. Hydroisomerization of *n*-decane over the Pd/ZSM-22 bifunctional catalysts: The effects of dynamic and static crystallization to the zeolite. Micropor Mesopor Mater 2019;274:1–8.

25. Zschiesche C, Himsl D, Rakoczy R, Reitzmann A, Freiding J, Wilde N, et al. Hydroisomerization of long-chain *n*-alkanes over bifunctional zeolites with 10-membered- and 12-membered-ring pores. Chem Eng Technol 2018;41:199–204.

26. Mehla S, Krishnamurthy KR, Viswanathan B, John M, Niwate Y, Kumar SAK, et al. *n*-Hexadecane hydroisomerization over BTMACl/TEABr/MTEABr templated ZSM-12. Micropor Mesopor Mater 2013;177:120–126.
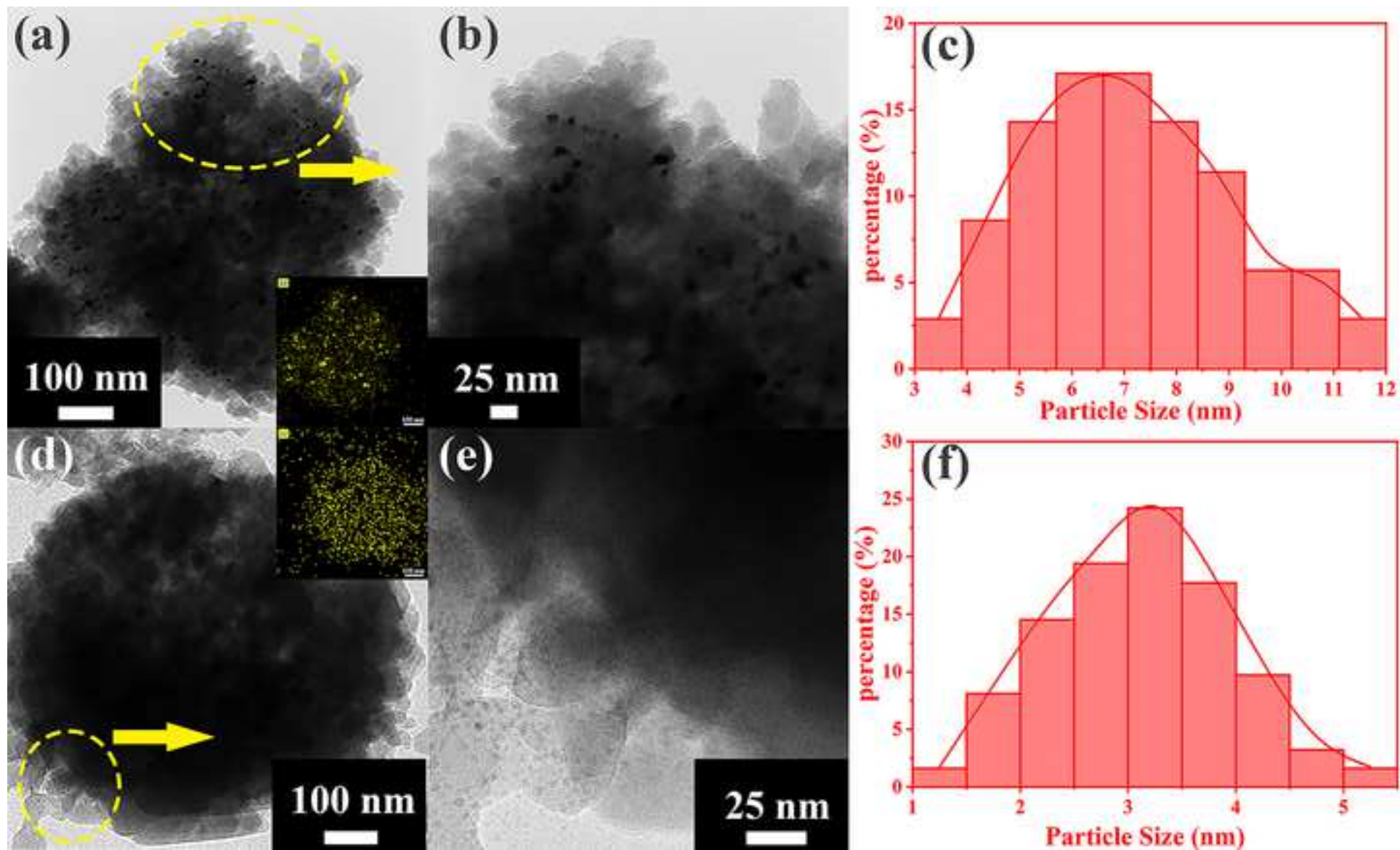
27. Tan Y, Hu W, Du Y, Li J. Species and impacts of metal sites over bifunctional catalyst on long chain *n*-alkane hydroisomerization: a review. Appl Catal A Gen 2021;611:117916.

28. Samad JE, Blanchard J, Sayag C, Louis C, Regalbuto JR. The controlled synthesis of metal-acid bifunctional catalysts: The effect of metal: acid ratio and metal-acid proximity in Pt silica-alumina catalysts for *n*-heptane isomerization. J Catal 2016;342:203–212.

29. Smirnova MY, Kikhtyanin OV, Smirnov MY, Kalinkin AV, Titkov AI, Ayupov AB, et al. Effect of calcination temperature on the properties of Pt/SAPO-31 catalyst in one-stage transformation of sunflower oil to green diesel. Appl Catal A Gen 2015;505:524–531.

30. Wang W, Liu C–J, Wu W. Bifunctional catalysts for the hydroisomerization of *n*-alkanes: the effects of metal-acid balance and textural structure. Catal Sci Technol 2019;9:4162–4187.

31. Batalha N, Pinard L, Bouchy C, Guillon E, Guisnet M. *n*-Hexadecane hydroisomerization over Pt-HBEA catalysts. quantification and effect of the intimacy between metal and protonic sites. J Catal 2013;307:122–131.

32. Karthikeyan D, Lingappan N, Sivasankar B, Jabarathinam NJ. Hydroisomerization of *n*-octane over bifunctional Ni-Pd/HY zeolite catalysts. Ind Eng Chem Res 2008;47:6538–6546.

33. Karakoulia S A, Heracleous E, Lappas A A. Mild hydroisomerization of heavy naphtha on mono-and bi-metallic Pt and Ni catalysts supported on Beta zeolite. Catal Today 2020;355:746–756.

34. Liu Y, Li Z, Yu Q, Chen Y, Chai Z, Zhao G, et al. A general strategy for fabricating isolated single metal atomic site catalysts in Y zeolite. J Am Chem Soc 2019;141:9305–9311.

35. Chen H, Yi F, Ma C, Gao X, Liu S, Tao Z, et al. Hydroisomerization of *n*-heptane on a new kind of bifunctional catalysts with palladium nanoparticles encapsulating inside zeolites. Fuel 2020;268:117241.

36. Wang Z, Zhang Y, Neyts EC, Cao X, Zhang X, Jang BWL, et al. Catalyst preparation with plasmas: how does it work?. ACS Catal 2018;8:2093–2110.

37. Nozaki T, Okazaki K. Carbon nanotube synthesis in atmospheric pressure glow discharge: a review. Plasma Process Polym 2008;5:300–321.
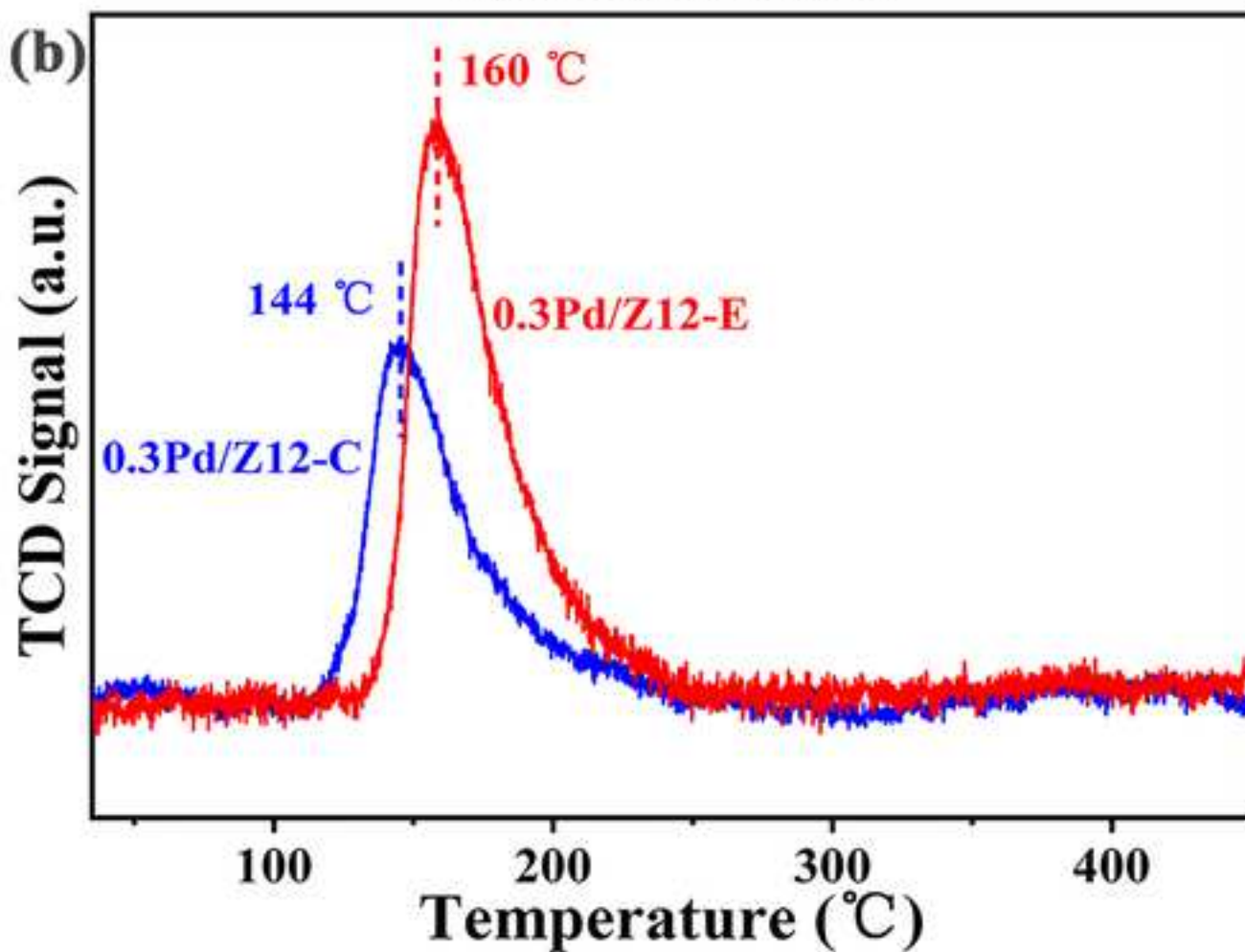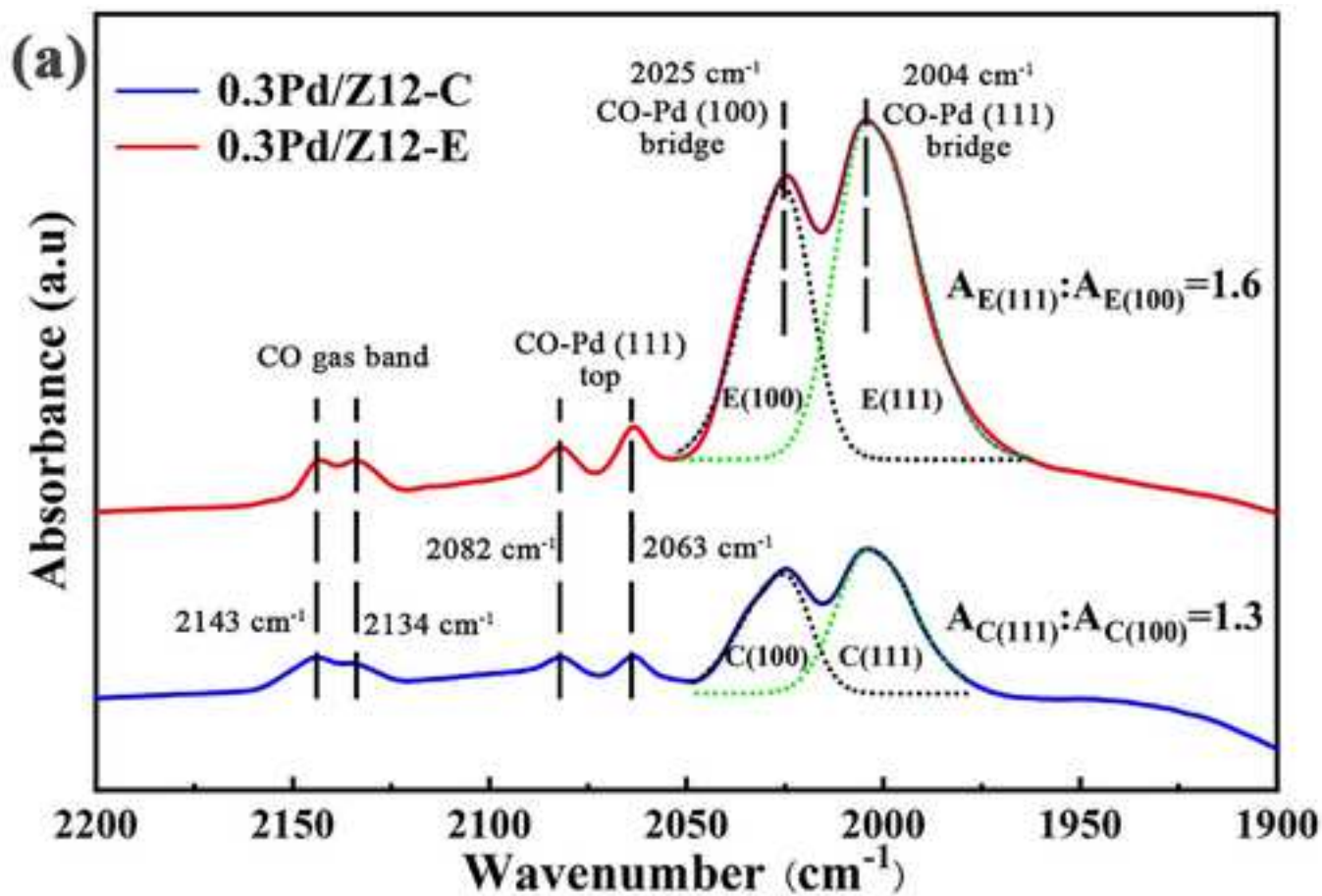
38. Wang W, Anderson CF, Wang Z, Wu W, Cui H, Liu C–J. Peptide-templated noble metal catalysts: syntheses and applications. Chem Sci 2017;8:3310–3324.

39. Chu W, Wang LN, Chernavskii PA, Khodakov AY. Glow-discharge plasma-assisted design of cobalt catalysts for Fischer-Tropsch synthesis. Angew Chem Int Ed 2008;47:5052–5055.

40. Li T, Wang W, Feng Z, Bai X, Su X, Yang L, et al. The hydroisomerization of *n*-hexane over highly selective Pd/ZSM-22 bifunctional catalysts: the improvements of metal-acid balance by room temperature electron reduction method. Fuel 2020;272:117717.

41. Emeis CA. Determination of integrated molar extinction coefficients for infrared absorption bands of pyridine adsorbed on solid acid catalysts. J Catal 1993;141:347–354.

42. Schmidt F, Hoffmann C, Giordanino F, Bordiga S, Simon P, Carrillo-Cabrera W, et al. Coke location in microporous and hierarchical ZSM-5 and the impact on the MTH reaction. J Catal 2013;307:238–245.

43. Zhang J, Maximov AL, Bai X, Wang W, Xiao L, Lin H, et al. Shape selectivity in hydroisomerization of *n*-hexadecane over Pd supported on zeolites: ZSM-22, ZSM-12 and Beta. Russ J Appl Chem 2020;93:1427–1437.

44. Zhang Y, Wang W, Jiang X, Su X, Kikhtyanin OV, Wu W. Hydroisomerization of *n*-hexadecane over a Pd–Ni_2P/SAPO-31 bifunctional catalyst: synergistic effects of bimetallic active sites. Catal Sci Technol 2018;8:817–828.

45. Wang W, Wang Z, Wang J, Zhong C–J, Liu C–J. Highly active and stable Pt–Pd alloy catalysts synthesized by room-temperature electron reduction for oxygen reduction reaction. Adv Sci 2017;4:1600486.

46. Tidahy HL, Hosseni M, Siffert S, Cousin R, Lamonier JF, Aboukais A, et al. Nanostructured macro-mesoporous zirconia impregnated by noble metal for catalytic total oxidation of toluene. Catal Today 2008;137:335–339.

47. Yang K, Wang B, Long C, Wang X. Synthesis and characterization of Pd–ZSM-23 with Na and H form for catalytic hydrodehalogenation of bromobenzene. Catal Commun 2008;9:431–436.

48. Ledwa KA, Kępinski L, Pawlyta M. Regenerability of complex $(PdO)_xPd_{0.05-x}Ce_{0.95}O_{2-y}$ catalyst stabilized on functionalized alumina surface. Mater Res Bull 2021;141:111357.
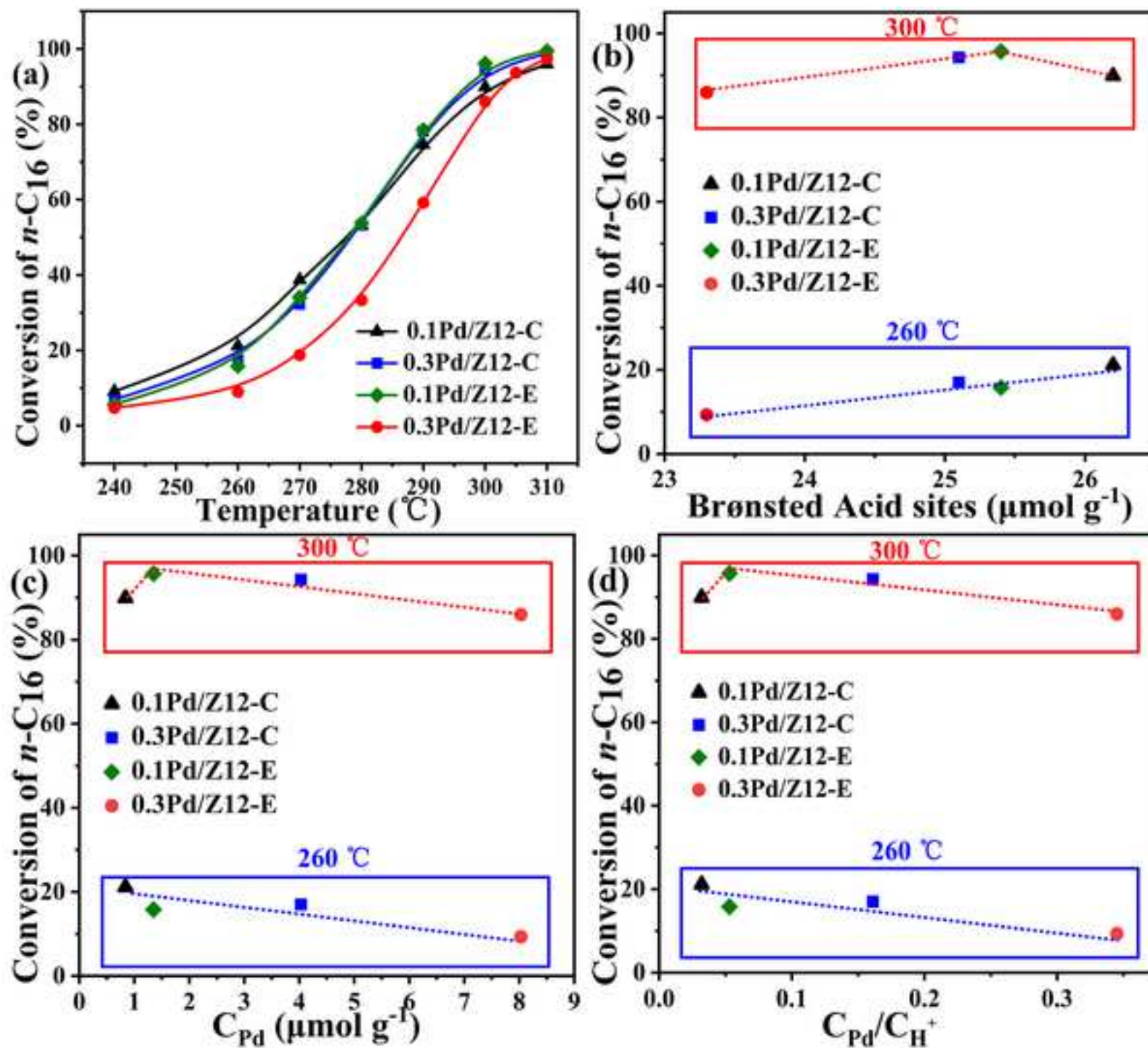
49. Canizares P, de Lucas A, Dorado F, Aguirre J. *n*-Butane hydroisomerization over Pd/HZSM-5 catalysts. Palladium loaded by ion exchange. Micropor Mesopor Mater 2001;42:245–254.

50. Aiken JD, Finke RG. A review of modern transition-metal nanoclusters: their synthesis, characterization, and applications in catalysis. J Mol Catal A Chem 1999;145:1–44.

51. Wang Y, Tao Z, Wu B, Xu J, Huo C, Li K, et al. Effect of metal precursors on the performance of Pt/ZSM-22 catalysts for *n*-hexadecane hydroisomerization. J Catal 2015;322:1–13.

52. Wang W, Wang Z, Yang M, Zhong C–J, Liu C–J. Highly active and stable Pt (111) catalysts synthesized by peptide assisted room temperature electron reduction for oxygen reduction reaction. Nano Energy 2016;25:26–33.

53. Lupescu JA, Schwank JW, Fisher GB, Hangas J, Peczonczyk SL, Paxton WA. Pd model catalysts: effect of air pulse length during redox aging on Pd redispersion. Appl Catal B Environ 2018;223:76–90.

54. Liu CJ, Zhao Y, Li Y, Zhang DS, Chang Z, Bu XH. Perspectives on electron-assisted reduction for preparation of highly dispersed noble metal catalysts. ACS Sustainable Chem Eng 2014;2:3–13.

55. Xia Y, Xiong Y, Lim B, Skrabalak SE. Shape-controlled synthesis of metal nanocrystals: simple chemistry meets complex physics?. Angew Chem Int Ed 2009;48:60–103.

56. Lim B, Jiang M, Tao J, Camargo PHC, Zhu Y, Xia Y. Shape-controlled synthesis of Pd nanocrystals in aqueous solutions. Adv Funct Mater 2009;19:189–200.

57. Kyriakou G, Boucher MB, Jewell AD, Lewis EA, Lawton TJ, Baber AE, et al. Isolated metal atom geometries as a strategy for selective heterogeneous hydrogenations. Science 2012;335:1209–1212.

58. Wang Y, Tao Z, Wu B, Chen H, Xu J, Yang Y, et al. Shape-controlled synthesis of Pt particles and their catalytic performances in the *n*-hexadecane hydroconversion. Catal Today 2016;259:331–339.

Figure 1
Click here to access/download;Figure;Figure 1.tif

Figure 2

Figure 2

Figure 3

Click here to access/download;Figure;Figure 3.tif ±

Figure 4

Click here to access/download;Figure;Figure 4.tif ⬇

(a)

- 0.3Pd/Z12-C
- 0.3Pd/Z12-E

2025 cm⁻¹
CO-Pd (100)
bridge

2004 cm⁻¹
CO-Pd (111)
bridge

$A_{E(111)}:A_{E(100)}=1.6$

CO gas band

CO-Pd (111)
top

E(100)   E(111)

2082 cm⁻¹   2063 cm⁻¹

2143 cm⁻¹   2134 cm⁻¹

C(100)   C(111)

$A_{C(111)}:A_{C(100)}=1.3$

Absorbance (a.u)

Wavenumber (cm⁻¹)

(b)

160 ℃

144 ℃

0.3Pd/Z12-E

0.3Pd/Z12-C

TCD Signal (a.u.)

Temperature (℃)

Figure 5   Click here to access/download;Figure;Figure 5.tif

Figure 7

Click here to access/download;Figure;Figure 7.tif ⬇

Figure 8

Figure 6

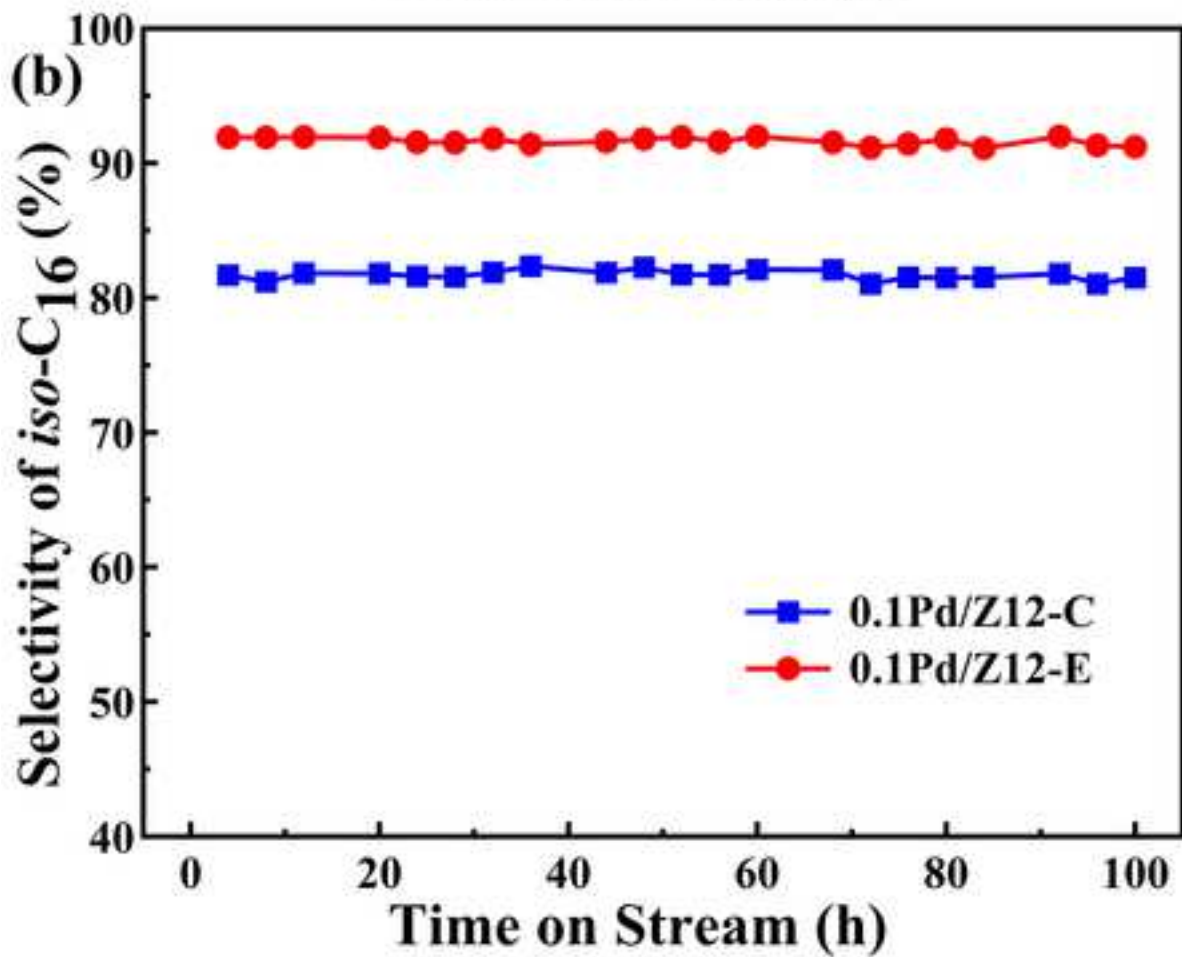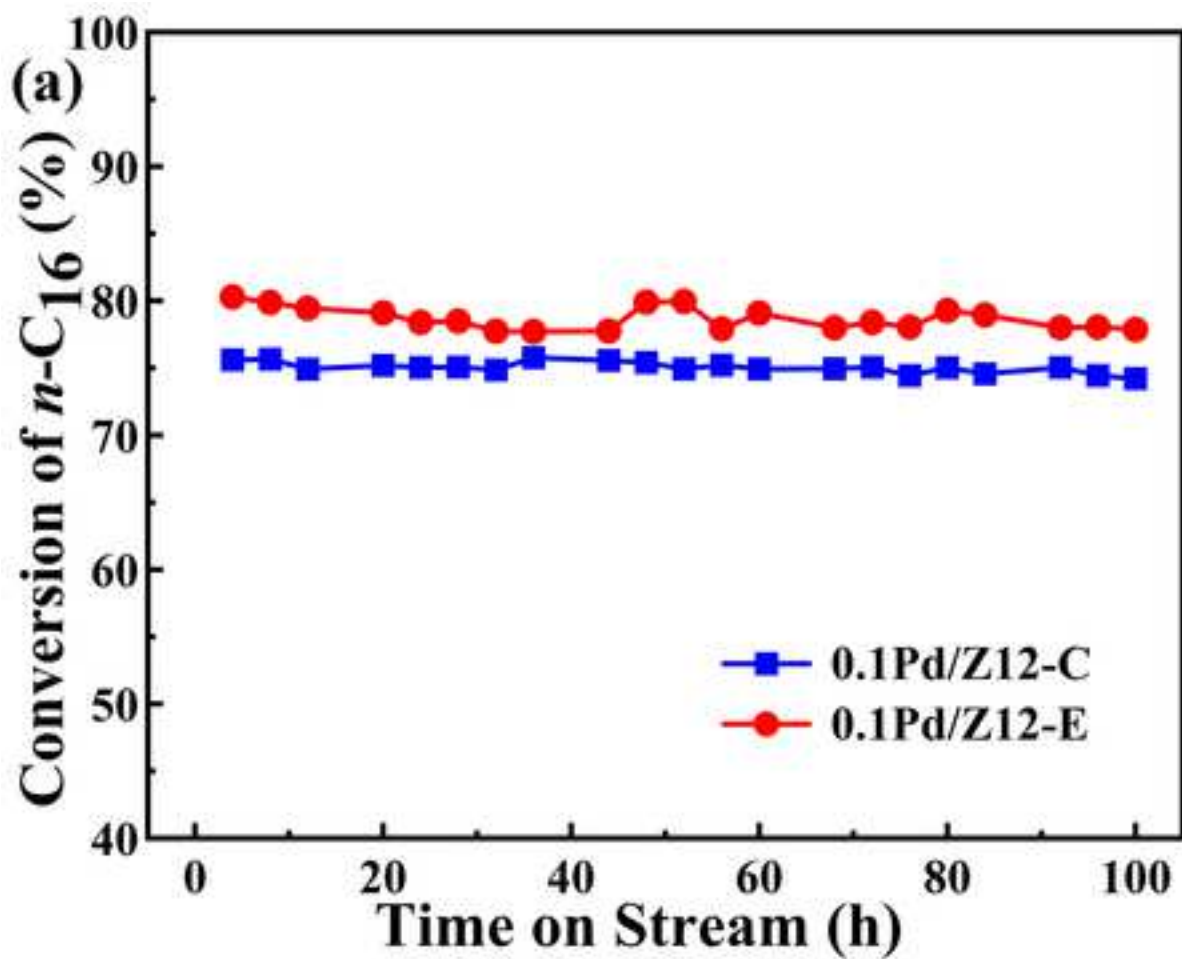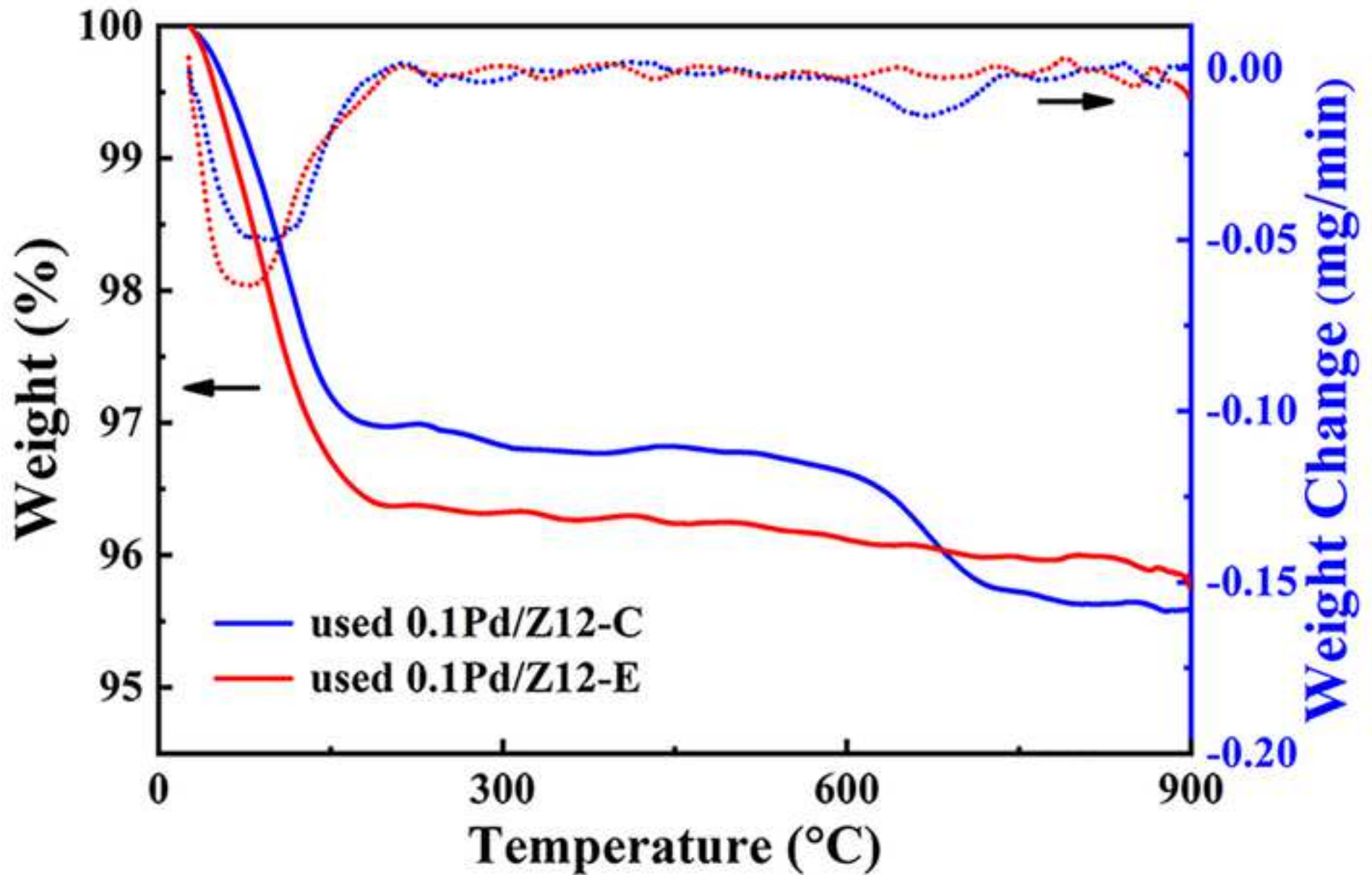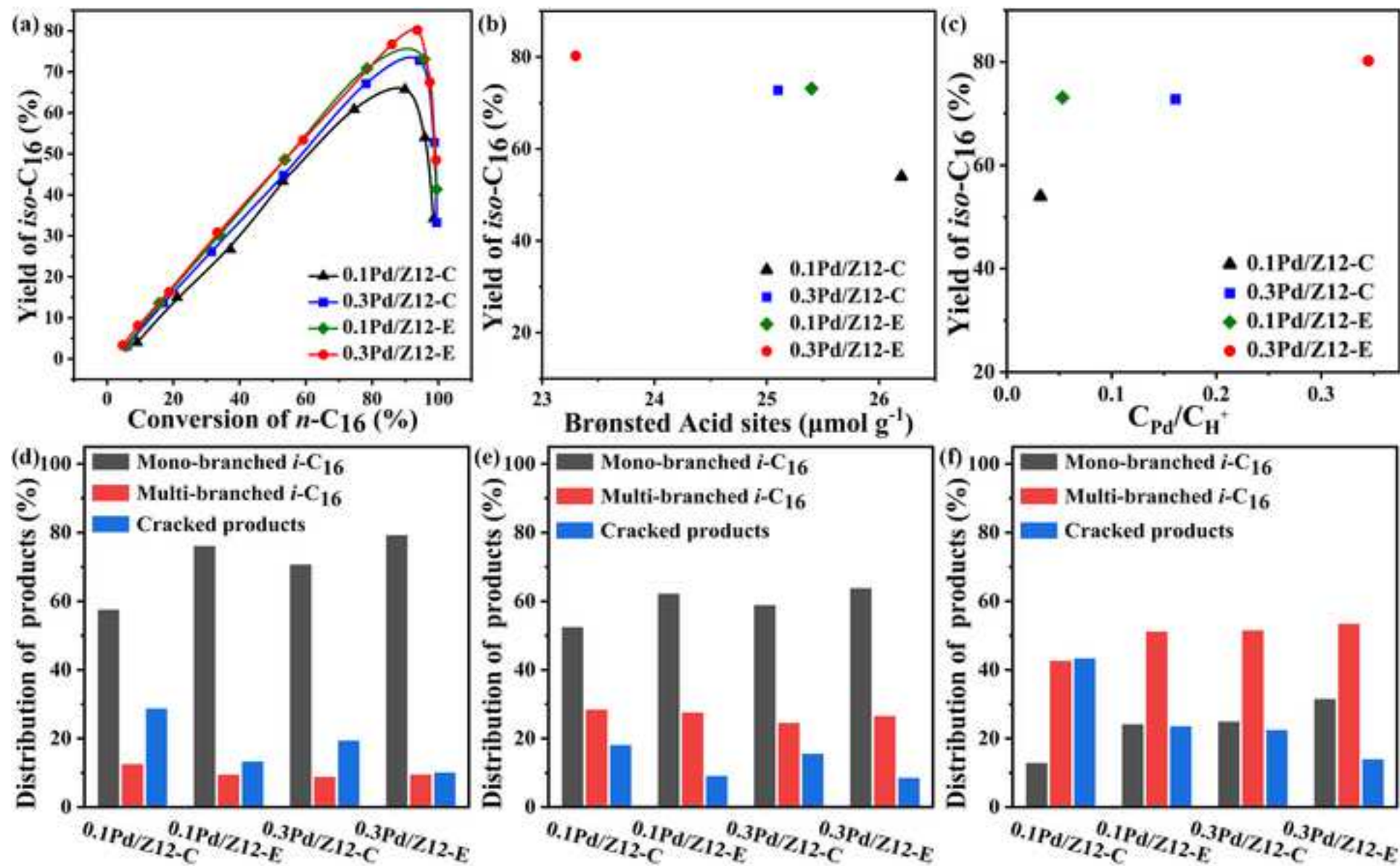Click here to access/download;Figure;Figure 6.tif

Table 1

Table 1. The textural properties of the ZSM-12 zeolite and all Pd/Z12 catalysts.

Sample	Relative crystallinity (%)	Surface area (m^2 g^{-1})			Pore volume (cm^3 g^{-1})		
		BET[a]	Micropore[b]	External	Total[c]	Micropore[b]	Mesopore
ZSM-12	100	345	285	60	0.243	0.113	0.130
0.1Pd/Z12-C	97	299	258	41	0.217	0.102	0.115
0.3Pd/Z12-C	82	261	221	40	0.217	0.088	0.129
0.1Pd/Z12-E	97	320	271	49	0.224	0.107	0.117
0.3Pd/Z12-E	82	294	245	49	0.221	0.097	0.124

Obtained by: [a] BET method, [b] t-plot method, [c] Volume adsorbed at $p/p_0 = 0.99$.

Table 2

Table 2. The Brønsted acid density and metal characteristics of ZSM-12 zeolite and

all Pd/Z12 catalysts.

Sample	Brønsted acid sites (μmol g^{-1})		D_{Pd} (%)[a]	C_{Pd} (μmol g^{-1})[b]	C_{Pd}/C_{H+}[c]	Pd size (nm)[d]
	Strong	Total				
ZSM-12	23.5	27.3	-	-	-	-
0.1Pd/Z12-C	22.0	26.2	8.9	0.84	0.032	12.5
0.3Pd/Z12-C	20.5	25.1	14.3	4.03	0.161	7.8
0.1Pd/Z12-E	21.1	25.4	14.4	1.35	0.053	7.8
0.3Pd/Z12-E	18.1	23.3	28.5	8.03	0.345	3.9

[a] Determined by H_2 chemisorption, [b] Calculated by Pd dispersion, [c] Calculated by total Brønsted acid sites, [d] Determined by the chemisorption method.

Click here to access/download
Supplementary Material
Supporting Information.docx

Graphical Abstract